ANL-84-38

ADVANCED FUEL CELL DEVELOPMENT

Progress Report for October – December 1983

by

R. D. Pierce, P. E. Blackburn, T. D. Claar,
R. J. Fousek, H. S. Huang, T. D. Kaun, N. Q. Minh,
J. R. Moreschi, F. C. Mrazek, J. J. Picciolo,
J. L. Smith, J. R. Stapay, and E. H. Van Deventer

ARGONNE NATIONAL LABORATORY, ARGONNE, ILLINOIS

Operated by THE UNIVERSITY OF CHICAGO
for the U. S. DEPARTMENT OF ENERGY
under Contract W-31-109-Eng-38

Distribution Category:
Energy Conversion
(UC-93)

ANL-84-38

ANL--84-38

DE85 000781

ARGONNE NATIONAL LABORATORY
9700 South Cass Avenue
Argonne, Illinois 60439

ADVANCED FUEL-CELL DEVELOPMENT

Progress Report for
October-December 1983

by

R. D. Pierce, P. E. Blackburn, T. D. Claar,* R. J. Fousek,*
H. S. Huang, T. D. Kaun, N. Q. Minh, J. R. Moreschi,
F. C. Mrazek, J. J. Picciolo,* J. L. Smith, J. R. Stapay,
and E. H. Van Deventer

Chemical Technology Division

August 1984

*Materials Science and Technology Division, ANL.

Blank Page

TABLE OF CONTENTS

LIST OF FIGURES

LIST OF FIGURES (contd)

LIST OF TABLES

ADVANCED FUEL CELL DEVELOPMENT

Progress Report for
October-December 1983

ABSTRACT

This report describes fuel cell research and development activities at Argonne National Laboratory (ANL) during the period October through December 1983. These efforts have been directed principally toward seeking alternative cathode materials to NiO for molten carbonate fuel cells. Based on an investigation of the thermodynamically stable phases formed under cathode conditions, a number of prospective alternative cathode materials have been identified. The materials $LiFeO_2$, Li_2MnO_3, and ZnO were selected from that list for investigation during this period. They have been doped to promote conductivity and tested for solubility and ion migration in the cell environment. The compound Li_2MnO_3 has proved most attractive, and techniques are being studied for the preparation of thin cathodes by tape casting the Li_2MnO_3 product.

SUMMARY

Cathode Development

Alternative Cathode Materials

Investigations were made of three alternative cathode materials: $LiFeO_2$, Li_2MnO_3, and ZnO. Tests were run to assess the effects of reaction gas (air versus CO_2-air) and salt composition (stoichiometric Li_2CO_3, excess Li_2CO_3, Li_2CO_3-K_2CO_3) on the conductivity of manganese-doped and undoped $LiFeO_2$. Material doped with one part manganese for each five parts iron was analyzed to be single-phase $LiFeO_2$ but to have a lattice parameter smaller than the 4.158 Å for undoped $LiFeO_2$. The results show that, contrary to our earlier conclusion, manganese doping at that level does not reduce the resistivity of the $LiFeO_2$. However, the composition of the reaction gas has a marked effect on the conductivity. Samples of doped or undoped $LiFeO_2$ were much more conductive if prepared under air than when produced under CO_2-air. Conductive material prepared under air became much less conductive during exposure to a CO_2-air/salt environment. Also, at 850°C $LiFeO_2$ had lower conductivity when excess Li_2CO_3 was present during the synthesis than when a stoichiometric quantity was employed. For 700°C syntheses, excess Li_2CO_3 did not decrease the conductivity of the product. In all cases, the conductive materials had slightly lower lattice parameters than the corresponding nonconductive samples.

Preliminary thermodynamic calculations were made to estimate the equilibrium extent of conversion of Fe_2O_3 to $LiFeO_2$ under the conditions of the several syntheses employed. Assuming ideal solid solutions of the Fe_2O_3 and $LiFeO_2$, the calculations indicate about 2% of the iron was unreacted for the CO_2-air syntheses and only 4 ppm was unreacted for the air syntheses.

Efforts have been made to produce a "large" batch of magnesium-doped Li_2MnO_3 to be used for cell testing. Analyses revealed that the doping had been successful, but the material was largely $LiMnO_2$. The incomplete oxidation of the manganese probably resulted from too deep a salt layer during the lithiation step; as a result, inadequate oxygen diffusion would have occurred during the reaction time allowed. The material was further exposed to lithium salt but with a shallower salt depth. Although most of the material is now Li_2MnO_3, the reaction still has not gone to completion except for a small portion that was reacted at the same time but in a separate small batch. These problems can be circumvented if satisfactory lithiation can be performed with stoichiometric, or only a slight excess of, Li_2CO_3 to avoid the totally flooded bed.

Tests were conducted to verify that in-cell lithium doping would not poison the conductivity observed for ZnO doped with Cr, Ga, and Zr. Experiments with lithium-doped ZnO exposed to cathode conditions verified the low level of in situ doping. The lithium dopant level dropped from 360 ppm to the 100 ppm value found earlier for ZnO that had not been doped with lithium before exposure to cathode conditions.

Because of the high levels of zinc transport observed with ZnO cathodes in migration tests, additional experiments with ZnO are not planned.

Stability Tests of Alternative Cathode Materials

Stability tests were made involving the synthesis of 14 oxides in the presence of Li_2CO_3-K_2CO_3 under a 1-atm pressure with four cathode gas (CO_2-H_2O-N_2-O_2-Ar) compositions. The materials Li_2MnO_3, $LiFeO_2$, and ZnO were stable for all four gas compositions.

An apparatus has been constructed for determining stable phases under a cover-gas pressure of 10 atm.

Cathode Materials Solubility Studies

Solubilities of potential cathode materials in Li_2CO_3-K_2CO_3 are being investigated using both direct melt sampling and cyclic voltammetry. Results were obtained for Li_2MnO_3, $LiFeO_2$, and ZnO as a function of temperature. The solubility of Li_2MnO_3 (about 1.5 wppm) in 70 mol % Li_2CO_3-K_2CO_3 under 50% CO_2-27% O_2-20% H_2O at 925 K is significantly lower than that for NiO (about 10 wppm); that of $LiFeO_2$ (about 9 wppm) is about the same as NiO; and that of ZnO (about 200 wppm) is rather high. The solubility of Li_2MnO_3 is relatively insensitive to H_2O and CO_2 content of the cover gas, but the solubility of ZnO increases with the H_2O and CO_2 content.

The solubilities of magnesium-doped Li_2MnO_3 are being examined. Initial results indicate that magnesium is being leached from the doped Li_2MnO_3. Under humidified 1/3 O_2-2/3 CO_2, 500-900 wppm magnesium was found in the carbonate equilibrated with this material. It is uncertain whether this magnesium was leached from the doped lattice or from unincorporated MgO dopant; because the solution saturated quickly, the latter is suspected. As found for undoped Li_2MnO_3, the level of manganese in the salt was low (<1.5 wppm).

For zirconium-doped ZnO, the ZnO solubility appears to increase with zirconium doping, from an average of 200 wppm zinc to about 300 wppm under humidified 1/3 O_2-2/3 CO_2. Less than 3 wppm zirconium was detected in the melt.

Cathode Material Migration

Cathode-material migration tests are run using small (37-mm dia) cells that incorporate the various alternative cathode materials. Results are obtained principally by posttest analysis of the electrolyte structure. Tests were completed with Li_2MnO_3, $LiFeO_2$, and ZnO cathodes in cells using 20% moisture in the electrode gases. No manganese was detected in the electrolyte from the Li_2MnO_3 cell. Iron found in the $LiFeO_2$ cell was comparable to the nickel observed in earlier tests with an NiO cathode. The zinc transported in the ZnO cell, however, was excessive and was found to be uniformly distributed throughout the electrolyte structure at a concentration more than ten times the solubility. The zinc appears to have combined with the $LiAlO_2$ in some manner.

In examining the electrolytes from these migration tests, significant quantities of chromium were found to have migrated into the electrolyte from the anode region--apparently from the Ni-10% Cr anode. This chromium transport was not noted in earlier migration tests in which the moisture content of the gases was lower.

Posttest analysis of $LiFeO_2$ and ZnO cathodes confirm that no phase changes or lattice parameter changes occurred under the cell operating conditions.

Fabrication of Cathode Structures

Work has continued to develop a spray-drying technique for synthesizing cathode materials. For the most successful runs, a slurry that was prepared by precipitating manganese and magnesium hydroxides from an aqueous nitrate solution was spray dried. The resultant powder of $Mg(OH)_2$, $Mn(OH)_2$, and $LiNO_3$ was heated overnight at 500°C and then calcined at 1000 or 1100°C in air for 24 h to form the doped Li_2MnO_3. The powder is being analyzed and the resistivity will be determined.

Work is continuing to produce tape-cast Li_2MnO_3 cathodes with tailored pore-size distributions. Tapes were prepared from two different Cerabind binders designed to produce high- and low-porosity material and with several different Li_2MnO_3 powders. The tapes were burned out, sintered, and analyzed. The sintering coarsened the Li_2MnO_3 excessively. The use of pore-former additions and less severe or no sintering will also be investigated.

Gas Cleanup Systems Analysis

An evaluation is being made of the feasibility of controlling the buildup of sulfur in molten carbonate fuel cells by the bleeding off of a portion of the anode exhaust rather than recycling it all to the cathode. This approach would have the detrimental effect of lowering the CO_2 content of the cathode gas. System performance analyses are being conducted to assess different bleed-off conditions. The first analyses are being done for natural gas-fired systems, where the impact on the CO_2 content will be more severe than for coal-based fuels, which have higher carbon contents.

I. INTRODUCTION

The advanced fuel cell studies at ANL are part of the DOE Advanced Fuel Cell Program. The objective of this DOE program is to reduce the technical uncertainties with fuel cells so that manufacturers and users can introduce high-efficiency generating systems, which have the capability of operating on coal or other fuels. At the present stage of development, the primary thrust of the ANL program is to provide supporting research and development that pursues fundamental understanding of fuel cell behavior and investigates alternative stack concepts.

The present molten carbonate fuel cells consist of a porous nickel anode, a porous lithiated nickel oxide cathode, an electrolyte structure that separates the anode and cathode and conducts only ionic current between them, and appropriate metal housings or, in the case of stacks of cells, intercell separator sheets. The cell housings (or separator sheets) bear upon the electrolyte structure to form a seal between the environment and the anode and cathode gas compartments. The usual electrolyte structure is a composite of discrete $LiAlO_2$ particles and a mixture of alkali metal carbonates. The carbonates are liquid at the cell operating temperature of about 925 K. At the anode, hydrogen and carbon monoxide in the fuel gas react with carbonate ion from the electrolyte to form water and carbon dioxide while giving up electrons to the external circuit. At the cathode, carbon dioxide and oxygen react and accept electrons from the external circuit to form carbonate ion, which is conducted through the electrolyte to the anode. In a practical cell stack, CO_2 for the cathode probably would be obtained from the anode exhaust.

It has become apparent that for pressurized operation, which is desirable for large power plants, nickel dissolution from the NiO cathode and deposition of metallic nickel in the electrolyte will prevent the attainment of the 4×10^4 h lifetime desired for commercial cells. The evaluation of possible alternative cathode materials is our principal current activity. We are also considering ways to obtain satisfactory cell life with NiO cathodes.

In addition to the cathode development efforts, cells are operated to assess the behavior of components and to understand the performance of life-limiting mechanisms at work within the cell. Cell operation is coupled with efforts on diagnostics and materials development.

II. CATHODE DEVELOPMENT

A. Alternative Cathode Materials

Because of the problem of NiO cathode dissolution in molten carbonate fuel cells (MCFCs), the MCFC research at ANL has concentrated principally on the investigation of alternative cathode materials. A number of oxides that are thermodynamically stable under cathode conditions have been identified as possible alternative cathode materials. During this quarter, the cathode development effort has been concentrated on the three most attractive materials studied to date: Li_2MnO_3, $LiFeO_2$, and ZnO.

1. $LiFeO_2$

a. Experimental
(N. Q. Minh, E. H. Van Deventer)

Experimental results presented in the previous quarterly report (ANL-84-9, p. 5) showed that the electrical conductivity of Mn-doped $LiFeO_2$, prepared by reaction of hydroxide coprecipitates of iron and manganese with carbonates (Li_2CO_3 or Li_2CO_3-K_2CO_3), depends on several preparation parameters such as temperature, carbonate reactant, and reaction gas. The effects of these parameters on the electrical conductivity of Mn-doped $LiFeO_2$ were investigated during this reporting period. For the purpose of comparison, the conductivity of undoped $LiFeO_2$ prepared under similar conditions was also measured. In addition, attempts were made to prepare Mn-doped material directly from iron oxide and manganese nitrate instead of from the hydroxide coprecipitates, since the coprecipitation procedure used is tedious and time-consuming.

A series of Mn-doped $LiFeO_2$ samples was prepared from Fe_2O_3 and $Mn(NO_3)_2$ by the following procedure. To begin, Fe_2O_3 powder was mixed with $Mn(NO_3)_2$ solution (Fe/Mn ratio: 5/1). The slurry was dried while stirring. Subsequent calcining and carbonate treatment steps produced three different pellets, which were then sintered in air at 1050°C for 1 h. The details of sample treatment along with the resultant effects on lattice parameters are presented in Table 1.

The resistivity of the three pellets is shown in Fig. 1. As can be seen from the figure, this preparation procedure did not produce good conducting Mn-doped $LiFeO_2$. Moreover, the sample prepared with stoichiometric amounts of Li_2CO_3 by the above procedure had much higher resistivity than that prepared by the coprecipitation method under similar conditions. Therefore, no further work on this preparation method is planned.

Preparation of a series of Mn-doped samples (nominal Fe/Mn ratio = 5/1) for conductivity measurements has been carried out by the coprecipitation method. Preparation parameters (no calcining step) and X-ray diffraction analysis of the samples are summarized in Tables 2 and 3. The electrical resistivity (ρ) results for Mn-doped $LiFeO_2$ samples are given in Figs. 2 and 3.

Table 1. Properties of Mn-Doped $LiFeO_2$ Samples Prepared from Iron Oxide and Manganese Nitrate

Sample No.	Calcining Step	Carbonate Treatment			XRD* Before Sintering/ After Sintering at 1050°C
		Carbonate	Temp., °C	Gas	
FM-1S1	None	Li_2CO_3-K_2CO_3	850	30% CO_2/ Air	$LiFeO_2$ 4.147Å/ $LiFeO_2$ 4.140A + minor $LiFe_5O_8$
FM-1S2	1000°C 60 h	Li_2CO_3-K_2CO_3	850	30% CO_2/ Air	$LiFeO_2$ 4.152Å/ $LiFeO_2$ 4.142A + minor $LiFe_5O_8$
FM-1S4	1000°C 60 h	Stoichiometric Li_2CO_3	850	Air	$LiFeO_2$ 4.14-4.15Å/a

[a]No results available for XRD after sintering.

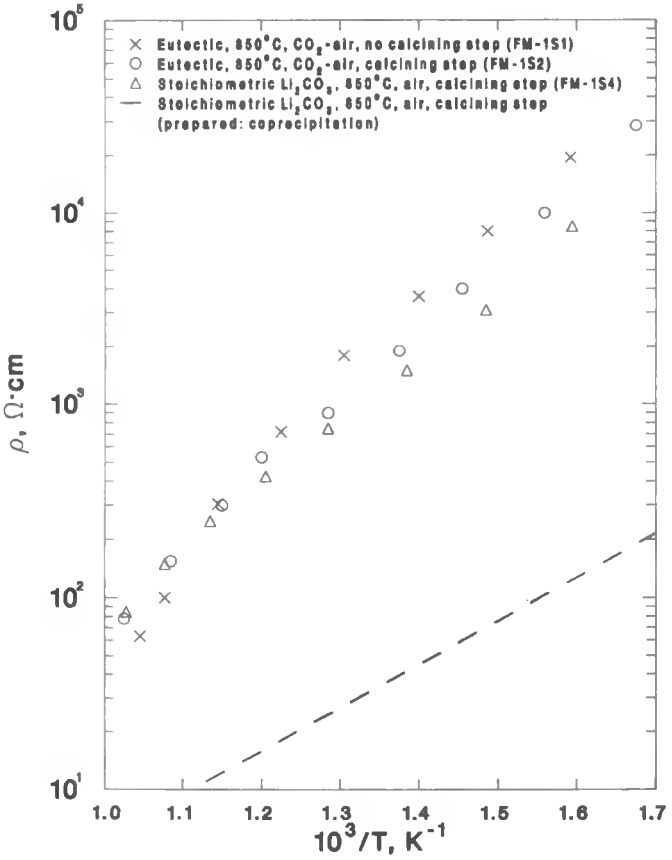

Fig. 1.

Resistivities of Mn-Doped $LiFeO_2$ Prepared from Fe_2O_3 and $Mn(NO_3)_2$

*Unless otherwise indicated, X-ray diffraction was done by B. Tani, Analytical Chemistry Laboratory (ACL).

Table 2. Properties of Mn-Doped $LiFeO_2$ Samples Prepared by the Coprecipitation Method at 700°C

Sample No.	Carbonate Treatment			XRD Before Sintering
	Carbonate	Temp., °C	Gas	
FM-3P4	Stoichiometric Li_2CO_3	700	30% CO_2/Air	$LiFeO_2$ 4.144Å, very minor Li_2MnO_3
FM-3P5	Excess Li_2CO_3 (3 times stoichiometric amount)	700	30% CO_2/Air	$LiFeO_2$ 4.144Å, very minor Li_2MnO_3
FM-1P3	Li_2CO_3-K_2CO_3	700	30% CO_2/Air	$LiFeO_2$ 4.144Å
FM-2P2	Stoichiometric Li_2CO_3	700	Air	$LiFeO_2$ 4.140Å

Table 3. Properties of Mn-Doped $LiFeO_2$ Samples Prepared by the Coprecipitation Method at 850°C

Sample No.	Carbonate Treatment			XRD Before Sintering/ After Sintering
	Carbonate	Temp., °C	Gas	
FM-2P4	Stoichiometric Li_2CO_3	850	30% CO_2/ Air	$LiFeO_2$ 4.146Å/
FM-2P5	Li_2CO_3-K_2CO_3	850	30% CO_2/ Air	$LiFeO_2$ 4.148Å/
FM-1P1	Stoichiometric Li_2CO_3	850	Air	$LiFeO_2$ 4.136Å/ $LiFeO_2$ 4.138Å
FM-3P1	Excess Li_2CO_3 (3 times stoichiometric amount)	850	Air	$LiFeO_2$ 4.136Å/
FM-2P3	Li_2CO_3-K_2CO_3	850	Air	$LiFeO_2$ 4.138Å

Samples of undoped $LiFeO_2$ were prepared by reacting Fe_2O_3 powder with Li_2CO_3 under conditions similar to those used for manganese doping. Details of the preparation conditions and X-ray diffraction results for undoped $LiFeO_2$ samples are shown in Tables 4 and 5. (Carbonate treatment was carried out for 60 h.) The conductivity of undoped $LiFeO_2$ samples is shown in Figs. 4-7.

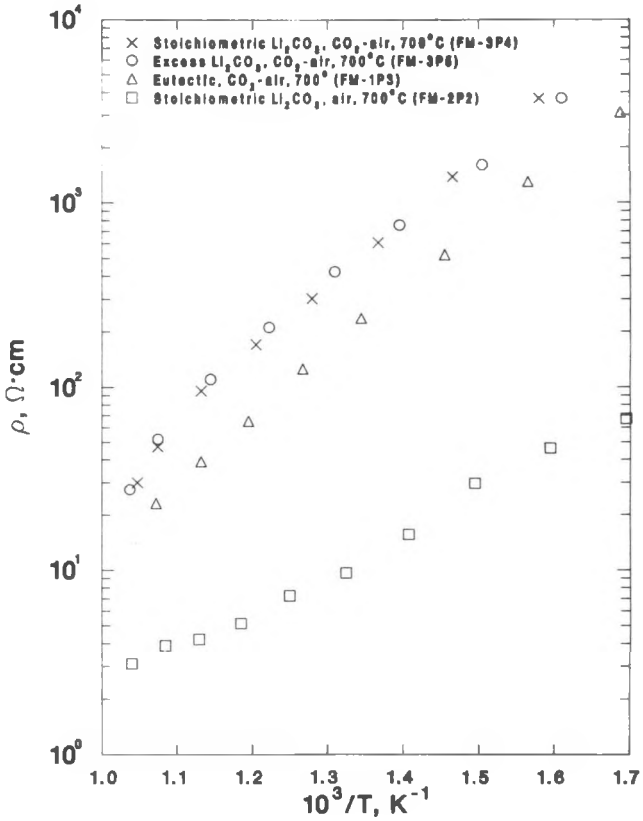

Fig. 2.

Resistivities of Four Pellets of Mn-Doped $LiFeO_2$

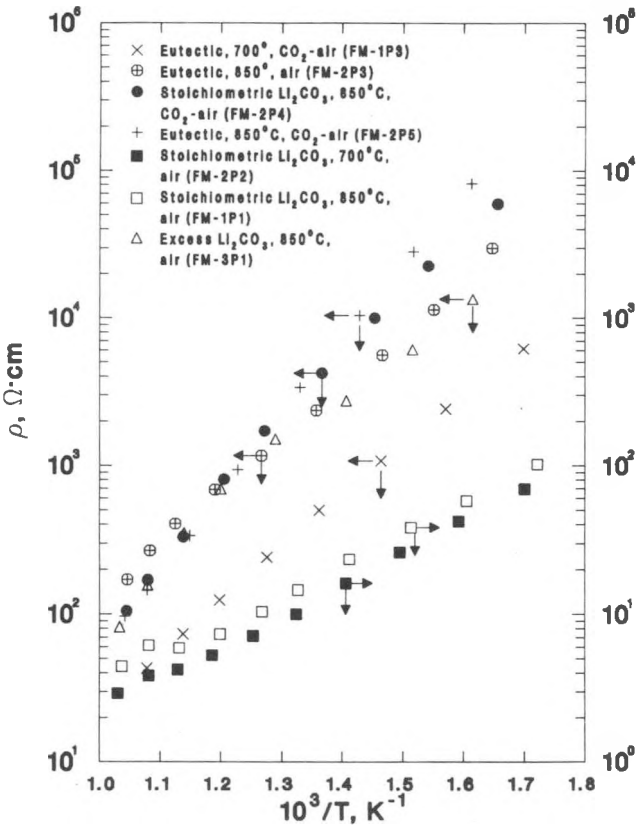

Fig. 3.

Resistivities of Seven Pellets of Mn-Doped $LiFeO_2$

Table 4. Properties of Undoped $LiFeO_2$ Prepared from Iron Oxide and Lithium Carbonate at 700°C

Sample No.	Carbonate	Carbonate Treatment		XRD Before Sintering
		Temp., °C	Gas	
F8	Stoichiometric Li_2CO_3	700	Air	$LiFeO_2$ 4.152 Å
F9	Excess Li_2CO_3	700	Air	$LiFeO_2$ 4.152 Å
F10	Li_2CO_3-K_2CO_3	700	Air	$LiFeO_2$ 4.156 Å
F11	Stoichiometric Li_2CO_3	700	30% CO_2/Air	$LiFeO_2$ 4.158 Å
F12	Excess Li_2CO_3	700	30% CO_2/Air	$LiFeO_2$ 4.158 Å
F13	Li_2O_3-K_2CO_3	700	30% CO_2/Air	$LiFeO_2$ 4.158 Å

Table 5. Properties of Undoped $LiFeO_2$ Prepared from Iron Oxide and Lithium Carbonate at 850°C

Sample No.	Carbonate Treatment			XRD Before Sintering/ After Sintering
	Carbonate	Temp., °C	Gas	
F3	Stoichiometric Li_2CO_3	850	30% CO_2/ Air	$LiFeO_2$ 4.157Å/
F1	Li_2CO_3-K_2CO_3	850	30% CO_2/ Air	$LiFeO_2$ 4.157Å/ $LiFeO_2$ 4.156 -4.152Å
F2	Stoichiometric Li_2CO_3	850	Air	$LiFeO_2$ 4.154Å/ LiFeO2 4.156Å
F5	Li_2CO_3-K_2CO_3	850	Air	$LiFeO_2$ 4.152Å/
F6	Excess Li_2CO_3 (3 times stoichiometric amount)	850	Air	$LiFeO_2$ 4.150Å/

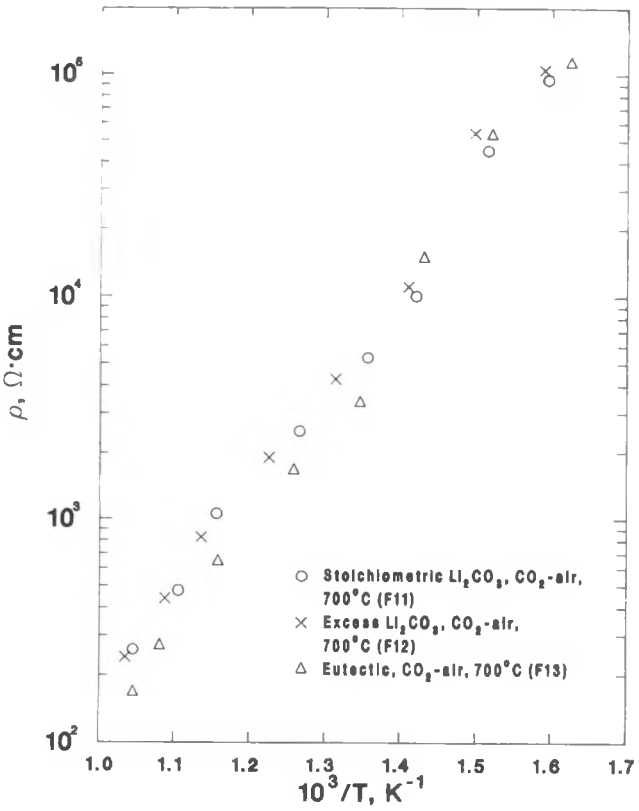

Fig. 4.

Resistivities of Undoped $LiFeO_2$ Prepared under CO_2/Air

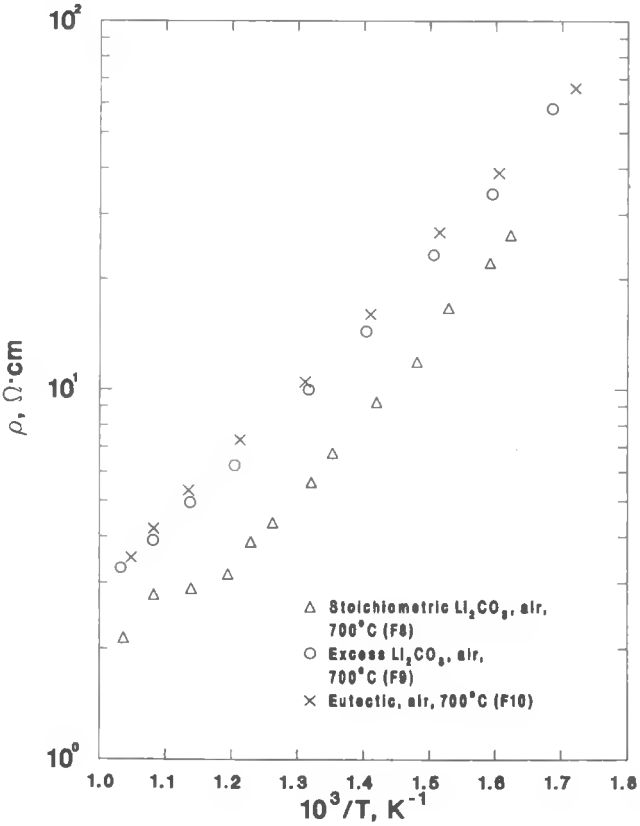

Fig. 5.

Resistivities of Undoped $LiFeO_2$ Prepared under Air

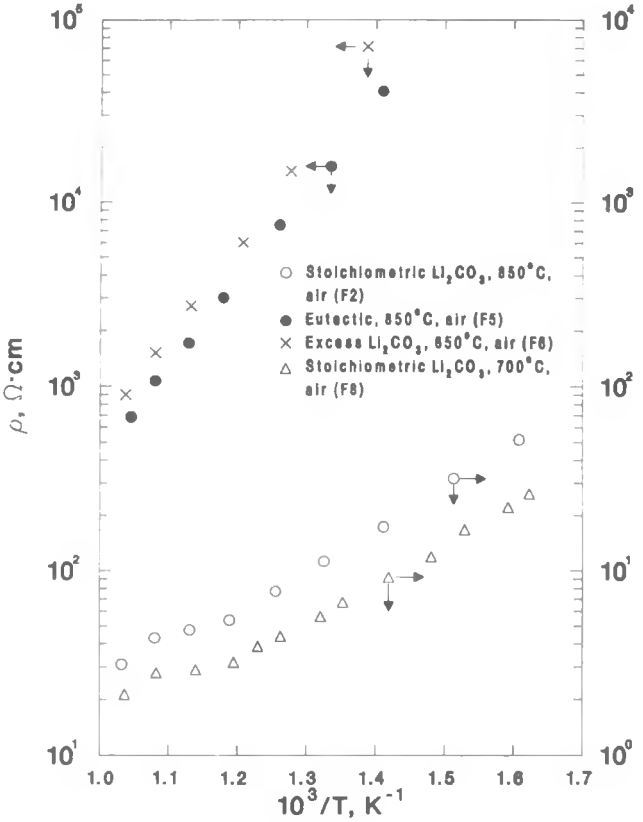

Fig. 6.

Resistivities of Undoped $LiFeO_2$ Prepared under Different Conditions

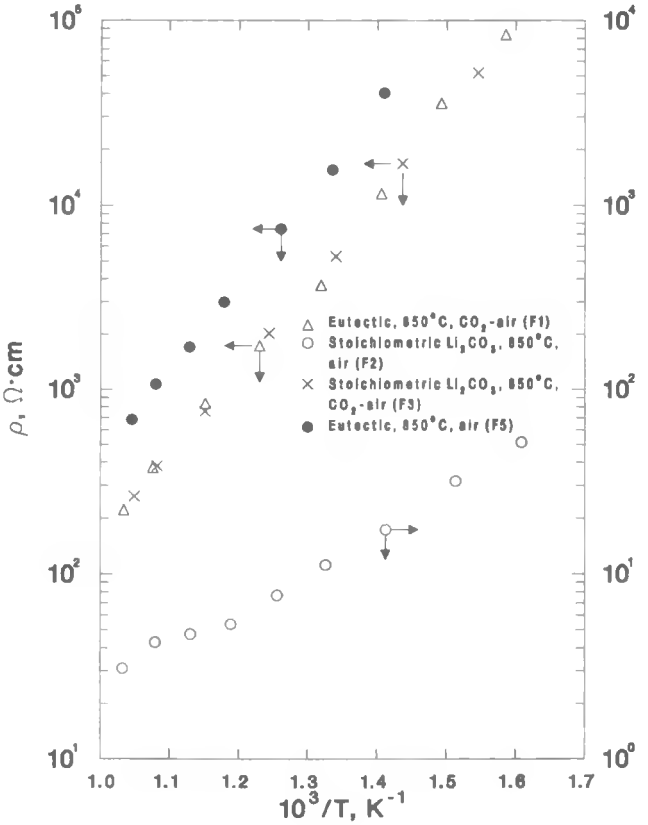

Fig. 7.

Resistivities of Undoped $LiFeO_2$ Prepared at 850°C in Air and CO_2-Air

From the results presented in Tables 2-5 and Figs. 2-7, the following conclusions can be drawn:

1. Manganese was successfully incorporated into the $LiFeO_2$ crystal lattice. The X-ray diffraction analyses indicate a decrease in lattice constant for Mn-doped samples, as compared with that for undoped samples (e.g., see Tables 2 and 4). However, it appears that Mn incorporation at this concentration level (Fe/Mn = 5/1) does not result in a decrease of the resistivity of $LiFeO_2$ prepared with stoichiometric amounts of Li_2CO_3 in air at 700 or 850°C. On the other hand, with the presence of excess Li_2CO_3 or Li_2CO_3-K_2CO_3 in the preparation at 700°C, resistivities of the prepared doped material were an order of magnitude smaller than those of the undoped material (e.g., see Figs. 2 and 4).

2. Preparation with stoichiometric amounts of Li_2CO_3 in air produces $LiFeO_2$ material with low resistivity. Excess Li_2CO_3 or Li_2CO_3-K_2CO_3 in the preparation at 850°C in air results in undoped $LiFeO_2$ material with much higher resistivity. However, it appears that excess Li_2CO_3 or Li_2CO_3-K_2CO_3 has no effect on resistivities of $LiFeO_2$ prepared under similar conditions at 700°C.

3. Reaction gas atmosphere has a marked effect on the electrical conductivity of $LiFeO_2$ materials prepared at 700°C. Figures 4 and 5 show that materials prepared under CO_2/air have much higher resistivities than those prepared under air. This effect is also observed for $LiFeO_2$ samples prepared at 850°C with stoichiometric amounts of Li_2CO_3. On the other hand, resistivities of $LiFeO_2$ prepared with either excess Li_2CO_3 or the Li_2CO_3-K_2CO_3 eutectic at 850°C appear to be the same and independent of reaction atmosphere (air or 30% CO_2/air).

An experiment was carried out to investigate whether conductive $LiFeO_2$ prepared in air is stable in the fuel cell cathode environment. A sample of undoped $LiFeO_2$ was prepared by reacting Fe_2O_3 powder with stoichiometric amounts of Li_2CO_3 in air at 700°C, followed by washing and sintering of the sample at 1050°C. The resistivity of the sintered sample is quite low, as shown in Fig. 8 (circles). The sample was then ground and treated in the Li_2CO_3-K_2CO_3 eutectic under 30% CO_2/air atmosphere for 100 h. The material was washed, pressed into a pellet, and resintered. Resistivity data taken on this pellet are given in Fig. 8 (crosses). It can be seen from the figure that, after the carbonate treatment under the cathode gas conditions, the resistivity of the sample increased several orders of magnitude, to about the same order of magnitude observed for $LiFeO_2$ prepared from Fe_2O_3 and Li_2CO_3-K_2CO_3 eutectic under similar cathode gas conditions.

The results obtained so far show that several samples of undoped $LiFeO_2$ prepared under certain conditions are quite conductive. The appreciable electronic conductivity suggests nonstoichiometry in those samples. The following two possibilities are recognized: (a) lithium deficiency (or iron excess), $Li_{1-x}Fe_{1+x}O_2$, and (b) lithium excess (or iron deficiency), $Li_{1+x}Fe_{1-x}O_2$. In case (a) the material exists as $Li^{+}_{1-x}Fe^{3+}_{1-x}Fe^{2+}_{2x}O_2$, which can be represented as a solid solution between $LiFeO_2$ and FeO. The lattice constant is 4.31 Å for FeO and 4.158 Å for stoichiometric $LiFeO_2$. Such a

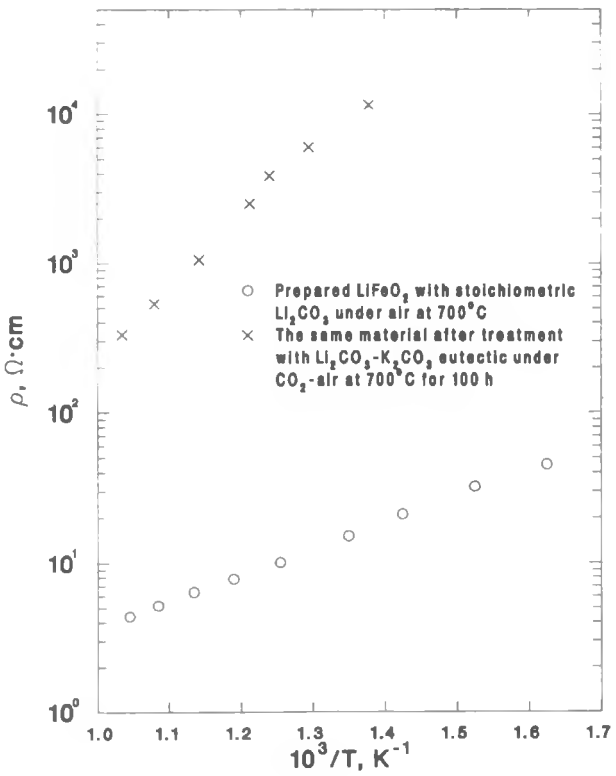

Fig. 8.

Resistivities of Undoped $LiFeO_2$ Prepared under Air before and after Carbonate Treatment under CO_2/Air

solid solution should, therefore, have a lattice parameter greater than 4.158 Å.[1] From Table 4 this is seen not to be the case for any specimen. Case (b) can be represented as $Li_{1+x}Fe^{3+}_{1-3x}Fe^{4+}_{2x}O_2$. Here a smaller unit cell dimension must be expected due to the smaller ionic radius of Fe^{4+}. Anderson and Schieber[2] and Demoisson et al.[3] indicate that nonstoichiometric materials of the type $Li_{1+x}Fe_{1-x}O_2$ can form, and the material has been shown to be semiconducting. X-ray diffraction of our conductive samples show a smaller lattice parameter than 4.158 Å, suggesting these samples are of the type $Li_{1+x}Fe^{3+}_{1-3x}Fe^{4+}_{2x}O_2$. Not enough information is available at present to give an explanation for the high resistivity observed for undoped $LiFeO_2$ samples (prepared in excess Li_2CO_3 or Li_2CO_3-K_2CO_3 under air at 850°C), although their lattice parameters are smaller than 4.158 Å.

Experiments on $LiFeO_2$ with low Mn dopant concentrations and on $LiFeO_2$ doped with zirconium are in progress.

b. Analytical
(P. E. Blackburn)

As reported above, large differences (3000-fold) have been observed between the resistivity of $LiFeO_2$ prepared in air and in 30% CO_2-air. Therefore, the effect of CO_2 pressure on the chemistry of the reaction

$$Li_2CO_3(\ell) + Fe_2O_3(s) \rightarrow 2LiFeO_2(s) + CO_2(g) \qquad (1)$$

was analyzed thermodynamically. This reaction was carried out experimentally at 700 and 850°C, where Li_2CO_3 is a liquid and $LiFeO_2$ and Fe_2O_3 are solids.

Some reactions were also carried out with a eutectic mixture of Li_2CO_3-K_2CO_3. This analysis, however, is limited to the 700°C measurements. The equilibrium constant for the reaction was calculated with NBS[4] thermodynamic values for $LiFeO_2$ and values of Barin and Knacke[5] for Li_2CO_3, Fe_2O_3 and CO_2. The doping with Mn_2O_3 was not considered in these calculations because it was found not to significantly affect the resistivity results.

Both $LiFeO_2$-Fe_2O_3 and Li_2CO_3-K_2CO_3 (when present) were assumed to form ideal solutions with unit activity coefficients. The constant for reaction (1) was calculated as

$$K = \exp [-16374/T + 70.14-7.24 \log (T)] \quad (2)$$

for $(A - x)Li_2CO_3 + (B - x)Fe_2O_3 = 2xLiFeO_2 + CO_2$, where the CO_2 pressure is fixed by the gas composition. In cases where $(C)K_2CO_3$ is present, it is assumed that K_2CO_3 decreases the activity of Li_2CO_3 but does not react with Fe_2O_3 or $LiFeO_2$.

An equation for x

$$x = B \left[\left(\frac{A - x}{A - x + C} \right) \Big/ \left(\frac{4P_{CO_2}}{K} + \frac{A - x}{A - x + C} \right) \right]^{1/2} \quad (3)$$

was derived. When no K_2CO_3 is present (C = 0),

$$x = B \Big/ \left(\frac{4P_{CO_2}}{K} + 1 \right)^{1/2} \quad (4)$$

When K_2CO_3 is present, Eq. 3 is solved by iteration, starting with x from Eq. 4. The mole fraction of the final constituents are

$$N_{K_2CO_3} = C/(C + A - x)$$

$$N_{Li_2CO_3} = (A - x)/(C + A - x)$$

$$N_{LiFe_2O_3} = 2x/(B + x)$$

$$N_{Fe_2O_3} = (B - x)/(B + x)$$

The calculated mole fraction of Fe_2O_3 assumed to dissolve in $LiFeO_2$ is compared to the resistivity measured by Minh (Section II.A.1.a) in Fig. 9. Both the resistivity and dissolved Fe_2O_3 increased markedly with the CO_2 present. The actual amount of Fe_2O_3 dissolved depends on solubility of Fe_2O_3 in $LiFeO_2$ and the Fe_2O_3 activity coefficient.

The effect of temperature on the solution of Fe_2O_3 in $LiFeO_2$ is shown in Fig. 10. The Fe_2O_3 solution decreases with increasing temperature. Minh (CMT) plans to make measurements at lower temperatures (<700°C) to see if the predicted effect of preparation temperature can be confirmed.

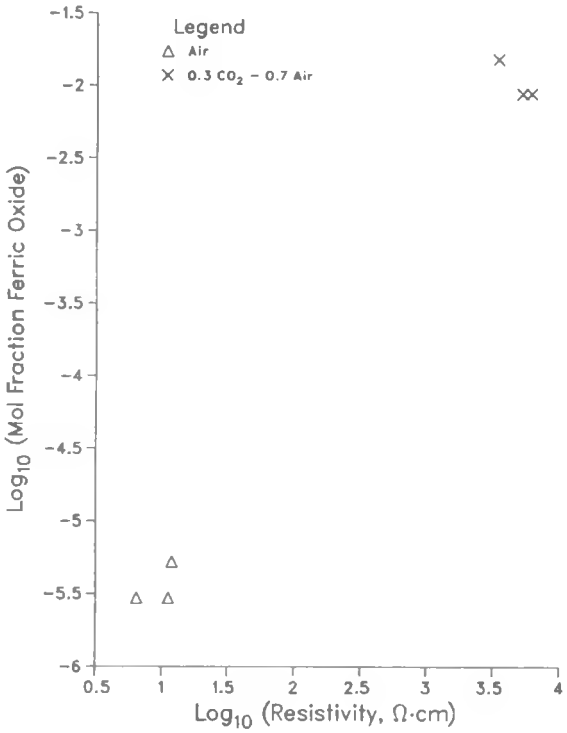

Fig. 9.

Correlation of Fe_2O_3 Solution in $LiFeO_2$ with Resistivity at 750°C (sample prepared at 700°C)

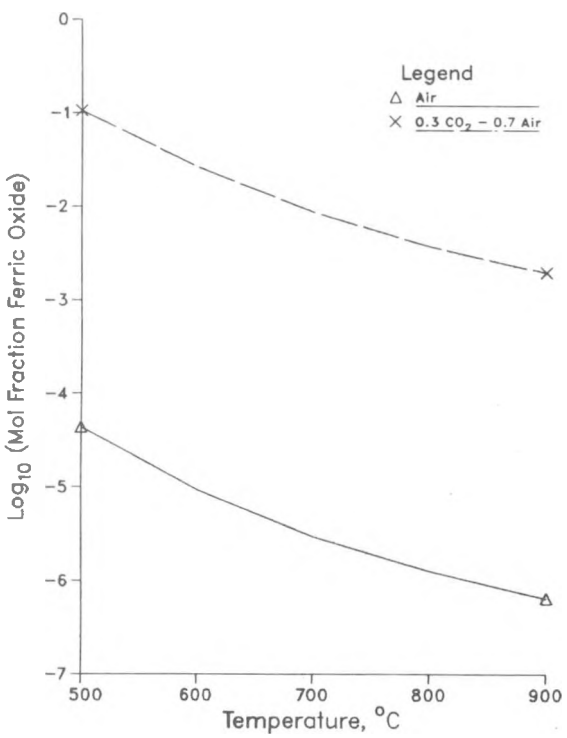

Fig. 10.

Calculated Fe_2O_3 Solution in $LiFeO_2$ as a Function of Temperature

2. Li_2MnO_3
(J. L. Smith)

An attempt was made to produce a large batch of Mg-doped Li_2MnO_3 by the usual procedure (ANL-83-89, p. 9) of coprecipitation and reaction with excess carbonates for 100 h at 700°C. The product was predominantly $LiMnO_2$ instead of Li_2MnO_3. This product was probably the result of the gas access to the reaction sites occurring only by diffusion through a relatively thick layer of liquid carbonates. The material was reacted twice more (100 h each time) in a large crucible to increase carbonate surface area exposed to the gas. The reaction went further but there was still a significant amount of $LiMnO_2$ remaining. The material was then reacted for 300 h but has not yet been analyzed.

This problem can be circumvented if it is shown that reaction with stoichiometric or slightly excess Li_2CO_3 produces the same product as reaction in a large excess of eutectic. If the coprecipitated material is reacted with a lesser amount of carbonates, the mass to be reacted will not be flooded and will allow better gas access to the reaction sites than the totally flooded mass that occurs when excess eutectic is used. The result will be faster reaction rates. This procedure would also greatly reduce another time-consuming step in the procedure--washing the excess carbonates. The possibility of changing the other major time-consuming procedure, filtering or centrifuging the sample after the precipitation and washing steps, is being explored.

3. ZnO
(N. Q. Minh)

Earlier results (ANL-84-9, p. 8) on doped ZnO had indicated that ZnO is a good electronic conductor with Cr, Ga, and Zr dopants. One concern is that when ZnO or doped ZnO is in contact with the carbonate electrolyte, lithium incorporation may occur to an extent that will cause a loss of conductivity. Experiments were performed to establish the equilibrium lithium-dopant concentration in ZnO in the cathode environment and to examine the effect of lithium incorporation on the conductivity of ZnO. The results obtained indicate a low level of lithium doping for undoped ZnO. Zirconium- and gallium-doped ZnO, after exposure to the carbonate, had a quite high lithium content, which we concluded was due to the presence of insoluble, lithium-containing compounds formed by the reaction between Li_2CO_3 and excess dopants.

Further results on the lithium incorporation for several doped and undoped ZnO samples are shown in Table 6. The doped ZnO samples were calcined at 1300°C. Attempts at sintering these samples into pellets for conductivity tests, following a carbonate treatment, were unsuccessful. The pellets did not sinter at temperatures up to 1100°C, where lithium vaporization becomes significant, and were too soft to be pressed into the conductivity measuring apparatus.

An experiment was carried out to establish the equilibrium lithium dopant concentration in ZnO under cathode gas conditions. Lithium doping was achieved by wet mixing, drying, and reacting lithium carbonate and zinc oxide

Table 6. Lithium Content of Undoped and Doped ZnO Exposed to Carbonate for 100 h under Cathode Gas Conditions (30% CO_2-air) at 700°C

Sample	Lithium Content,[a] ppm		
	1	2	3
Undoped ZnO	169	166	144
2 mol % Cr_2O_3-ZnO	443		
1 mol % Ga_2O_3-ZnO	1267		
3 mol % ZrO_2-ZnO	1943		

[a]Analysis performed by I. Fox, ACL.

for about 10 h at 1000°C. The material was then washed free of excess Li_2O. X-ray diffraction analysis indicated ZnO with no extra lines in the pattern. Chemical analysis showed a lithium content of 364 ppm, which was lower than expected; however, it was adequate for testing purposes. Some of this lithium-doped ZnO material was exposed to the carbonate eutectic under a cathode gas atmosphere (30% CO_2-air) for 100 h at 700°C. The material was then washed. Analysis of the washed material showed the lithium content had dropped to 99 ppm, which is about the same observed for undoped ZnO exposed to the carbonate under similar conditions. This result confirms an equilibrium lithium dopant level on the order of 100 ppm in ZnO in contact with Li_2CO_3-K_2CO_3 eutectic at 700°C under the 30% CO_2-air atmosphere. A few additional experiments on the effect of lithium incorporation on the conductivity of doped and undoped ZnO were run, and analyses are in progress. No additional experiments are planned with ZnO because of observed high solubility and excessive in-cell migration (see Sections II.C and D).

B. Stability Tests of Alternative Cathode Materials

(E. H. Van Deventer and J. R. Moreschi)

Stability tests to identify possible cathode materials have been completed to determine the stable phases in various cathode environments. In these tests, fourteen candidate materials in contact with Li_2CO_3-K_2CO_3 eutectic were exposed to various gas compositions (Table 7) for 100 h at atmospheric pressure and 700°C. The results of posttest X-ray diffraction analyses of these materials are listed in Table 8. The three alternative cathode materials (Li_2FeO_2, Li_2MnO_3, and ZnO) studied this quarter were stable for all four gas compositions.

The foregoing tests were done with an apparatus that simulated MCFC operating conditions except that elevated pressures (up to 10 atm) were not used. Accordingly, an apparatus was designed to test materials under conditions which more closely simulate extreme operating conditions. Provisions were also made to study which compounds might be stable under anode conditions. This apparatus has been constructed, passed safety inspections, and is now operational.

Table 7. Cathode Gas Compositions

Run	Composition, mol %				
	CO_2	H_2O	N_2	O_2	Ar
AC-EG	3.4	5.3	76.7	14.6	-
CG-1	12.9	40.7	44.5	1.9	-
CG-2	17.1	5.0	63.4	13.8	0.7
CG-3	21.8	17.9	47.1	12.6	0.6

Since anode and cathode gases typically contain significant amounts of water, the apparatus uses a high-pressure liquid chromatography pump as a means of injecting water into the flowing gas streams. Thus far, this device seems to be performing its designed task satisfactorily.

C. Cathode Materials Solubility Studies
(T. D. Kaun)

The excessive solubility of lithiated NiO prompted a search for alternative cathode materials. Low solubility of cathode material is necessary to maintain the desired cathode microstructure of a carbonate-wetted gas-diffusion electrode. Equilibrium solubility data are of added interest in predicting cell stability with alternative cathode materials under various operating conditions. In addition, solubility data are valuable to support cathode material migration tests (see Section II.D).

Initial solubility tests were completed for the three alternative cathode materials--Li_2MnO_3, $LiFeO_2$, and ZnO. Figure 11 is provided for comparing the solubility of these materials from available data at temperatures of 823-1023 K. With cathode gas conditions of 1/3 O_2-2/3 CO_2 humidified with 330 K H_2O (~20% H_2O in gas), Li_2MnO_3 has the lowest solubility, with a median value of 1.5 wppm Mn. Solubility of Li_2MnO_3 is considered to be in the targeted range for long-term cathode stability (40,000 h). The solubility of $LiFeO_2$ had a median value of 10 wppm Fe, which is slightly lower than NiO, but is still in a questionable range for long-term cathode stability. (Our particular test examined Zn-doped $LiFeO_2$; undoped material will be examined.) Solubility of ZnO appears excessive for long-term cathode application, with a median value of 200 wppm. Under other cathode conditions such as dry gas, these three materials exhibit the same relative rankings for solubility level.

Additional concerns in the evaluation of alternative materials are being addressed. High solubility of dopant material could lead to dopant leaching of the cathode material. Also, preliminary data indicated that the $LiAlO_2$ electrolyte matrix material may serve as a sink for cathode material solubility products.

Table 8. Stable End Products as Identified by XRD

Run	Material Charged													
	Fe_2O_3	Fe_3O_4	Ga_2O_3	MgO	MnO_2	Nb_2O_5	SnO_2	Ta_2O_5	TiO_2 (anatase)	TiO_2 (rutile)	V_2O_5	WO_3	ZnO	ZrO_2
CG-3	α-$LiFeO_2$	—	—	MgO $Mg(OH)_2$	Li_2MnO_3	—	Li_2SnO_3 SnO_2	Li_3TaO_4 a	—	Li_2TiO_3	Li_3VO_4	K_2WO_4	ZnO	Li_2ZrO_3 ZrO_2 a
CG-2	α-$LiFeO_2$	$LiFe_5O_8$[b] α-$LiFeO_2$ Fe_3O_4 Fe_2O_3	not identified	MgO $Mg(OH)_2$ a	Li_2MnO_3	Li_3NbO_4 $KNbO_3$	Li_2SnO_3 SnO_2	Li_3TaO_4 a	Li_2TiO_3	Li_2TiO_3	Li_3VO_4	—	ZnO	Li_2ZrO_3 ZrO_2 a
CG-1	γ-$LiFeO_2$	α-$LiFeO_2$	$LiGaO_2$ a	MgO $Mg(OH)_2$	Li_2MnO_3 $LiMnO_2$	Li_3NbO_4 $KNbO_3$ a	Li_2SnO_3 SnO_2	Li_3TaO_4 a	Li_2TiO_3	Li_2TiO_3	Li_3VO_4	—	ZnO	Li_2ZrO_3 ZrO_2 a
AC-EG	α-$LiFeO_2$	α-$LiFeO_2$	$LiGaO_2$ a	MgO	Li_2MnO_3	Li_3NbO_4 $KNbO_3$ a	Li_2SnO_3 SnO_2	Li_3TaO_4 a	Li_2TiO_3	Li_2TiO_3	Li_3VO_4	K_2WO_4	ZnO	Li_2ZrO_3 ZrO_2 a

[a] Unidentified phase(s) present.

[b] The magnetite used in this run was from a natural ore.

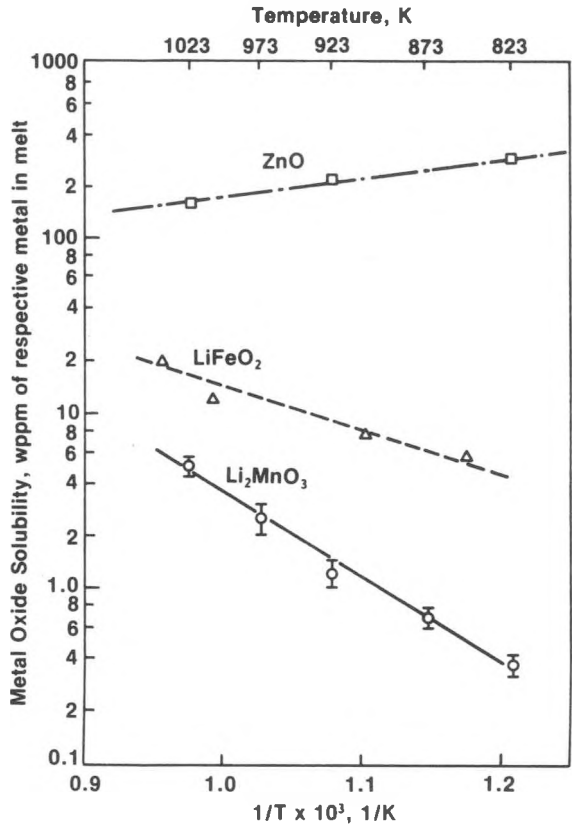

Fig. 11.

Solubilities of Alternative Cathode Materials in 70 mol % Li_2CO_3-K_2CO_3 as a Function of Temperature in the Presence of 330 K Humidified 1/3 O_2-2/3 CO_2

1. ZnO Solubility

As in previous solubility examinations,[6] the ZnO tests used cyclic voltammetry coupled with physical sample analysis. The cyclic voltammograms were controlled in the voltage range of +0.2 V to -1.2 V vs. the reference electrode of 1/3 O_2-2/3 CO_2 on gold. Introduction of ZnO into the carbonate melt produced anodic and cathodic peaks at about -0.9 V, as shown in Fig. 12. Physical samples from the melt were analyzed by Inductively Coupled Plasma/Atomic Emission Spectroscopy (ICP/AES)* by a preparation method that selectively dissolves $ZnCO_3$ in the presence of ZnO. The carbonate samples were dissolved by bubbling CO_2 into H_2O and were subsequently filtered to eliminate ZnO contamination (further described in the last quarterly report, ANL-84-9, p. 19).

Zinc oxide solubility in 70 mol % Li_2CO_3-K_2CO_3 was determined by the above methods for the temperature range of 823-1023 K. Figure 13 provides ZnO solubility results for both a dry and a humidified (330 K H_2O for 20% H_2O gas) gas condition. For the dry condition, ZnO solubility decreases with temperature: from 170 wppm Zn in the carbonate eutectic at 823 K to 110 wppm Zn at 1023 K. Humidified gas increases overall ZnO solubility: from 270 wppm Zn at 823 K to 140 wppm Zn at 1023 K. A datum of the pot-type solubility study with dry 30% CO_2-air gas indicated 75 wppm Zn level at 923 K. Carbon dioxide partial pressure appears to affect strongly the solubility of ZnO in molten carbonates.

*Analytical results by E. Huff and A. Essling, ACL.

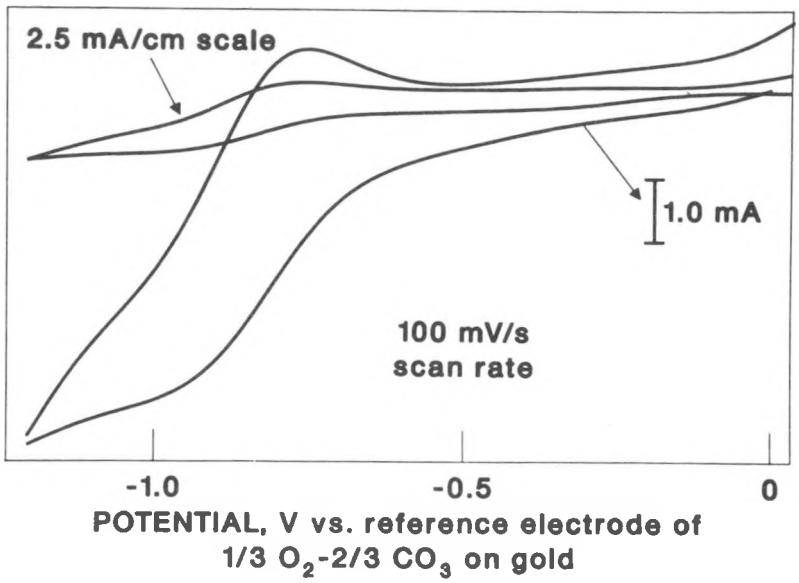

Fig. 12. Cyclic Voltammogram of ZnO-Containing Melted Carbonate (70 mol % Li_2CO_3-K_2CO_3) at 923 K under Humidified (20% H_2O) 1/3 O_2-2/3 CO_2 Cathode Gas

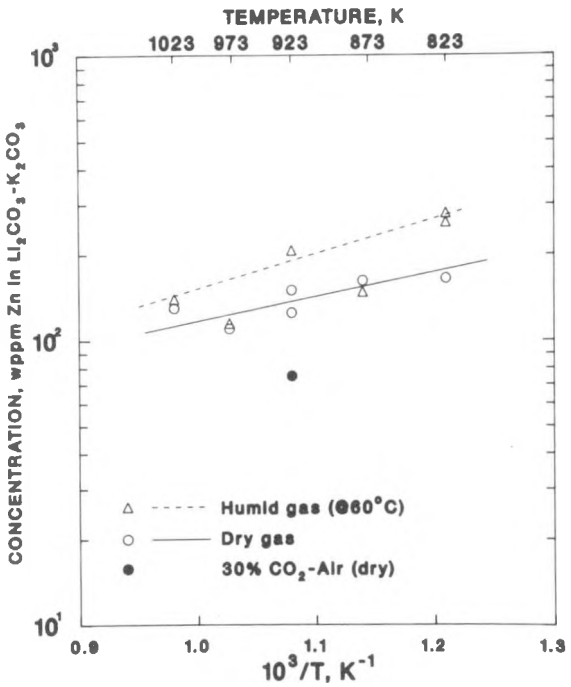

Fig. 13.

Solubility of ZnO in 70 mol % Li_2CO_3-K_2CO_3 under 1/3 O_2-2/3 CO_2 Gas (unless noted)

2. Solubility of Doped Cathode Materials

The alternative cathode materials Li_2MnO_3, $LiFeO_2$, and ZnO have been examined for the effects of temperature, humidity, and electrolyte composition on solubility. These materials require doping to impart sufficient electrical conductivity necessary for the fuel cell cathode. Solubility tests for the doped alternative cathode materials are under way. Leaching of dopant could cause degradation of cell performance due to altered conductivity. Two candidates for cathode application, Mg-doped Li_2MnO_3 and Zr-doped ZnO, were investigated in this report period.

a. Mg-Doped Li_2MnO_3

The solubility of MgO was examined in preparation for a test of Mg-doped Li_2MnO_3. A piece of dense MgO was used for this solubility test. Microscopic examination (by F. C. Mrazek, CMT) of this MgO material by reflected light and scanning electron microscopy (SEM) revealed no second phase, thus suggesting a high-purity material. The solubility tests revealed rather high levels of Mg in the carbonate (70 mol % Li_2CO_3-K_2CO_3) under humid (20% H_2O) 1/3 O_2-2/3 CO_2 gas. In the temperature range 823-1023 K, solubility decreased slightly with temperature from 790 to 600 wppm Mg in the carbonate (Fig. 14). Under a humid cathode gas, the Mg levels arising from solubility of Mg-doped Li_2MnO_3 were even slightly higher, 500 to 900 wppm Mg over the temperature range 823-1023 K. The results also indicated a somewhat increased Mg level due to humidity. In dry cathode gas, the Mg level from Mg-doped Li_2MnO_3 was ≤600 wppm Mg at all temperatures tested. It is likely that the observed level of Mg in these tests was introduced from unincorporated Mg dopant, because the solution saturated rather quickly.

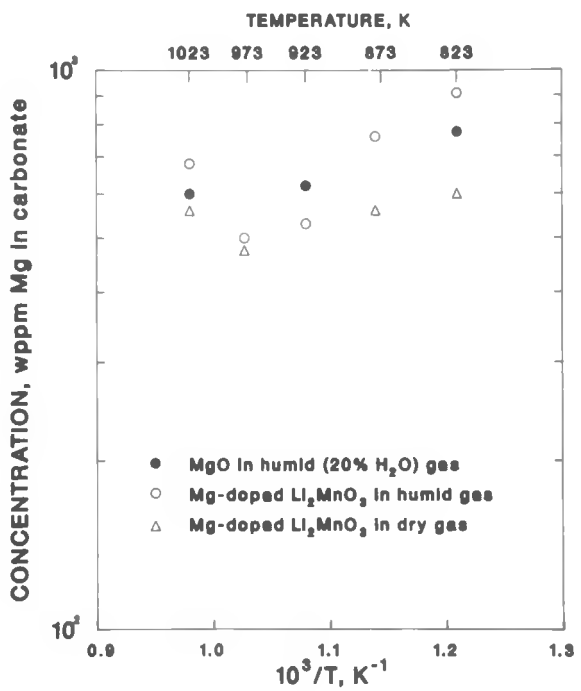

Fig. 14.

Solubility Tests of MgO and Mg-Doped Li_2MnO_3 in 70 mol % Li_2CO_3-K_2CO_3 and 1/3 O_2-2/3 CO_2 Cathode Gas

The Mn levels in the carbonates arising from solubility of the Mg-doped Li_2MnO_3 were similar to the results for the undoped material. The available data indicated 3.0 wppm Mn present at 973 K and 1.4 wppm Mn at 923 K.

b. Zr-Doped ZnO

Initial results of solubility tests on Zr-doped ZnO indicated low zirconium levels, <3 wppm Zr in the 70 mol % Li_2CO_3-K_2CO_3 melt for both humid (20% H_2O) and dry 1/3 O_2-2/3 CO_2 cathode gas. The Zn levels present were quite high, similar to undoped ZnO. Values of 140 wppm Zn were obtained for the solubility tests with dry cathode gas. Under humid gas, Zn levels arising from the solubility of Zr-doped ZnO were approximately 50% greater than those for undoped ZnO, with a median value of 300 wppm Zn (Fig. 15). This is our first observation that dopant may have affected the solubility of the parent material. Certain dopants may reduce the solubility of some materials in carbonates.

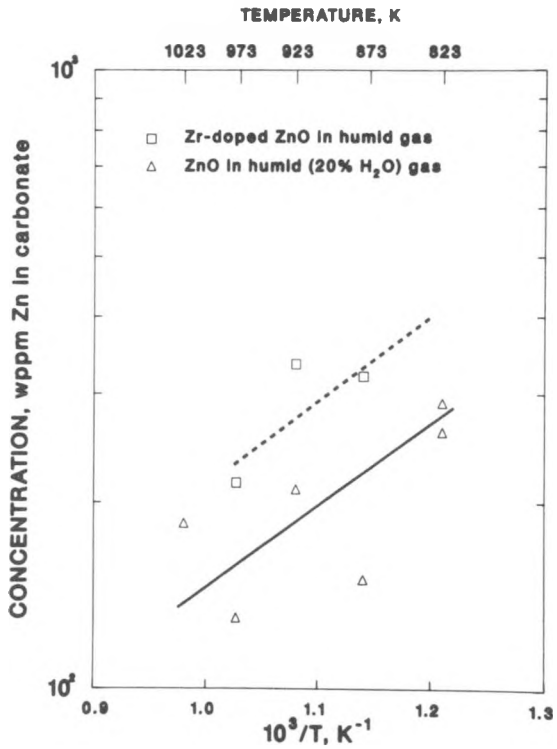

Fig. 15.

Solubility of ZnO and Zr-Doped ZnO in 70 mol % Li_2CO_3-K_2CO_3 and 1/3 O_2-2/3 CO_2 Cathode Gas Humidified with 330 K Water

D. Cathode Material Migration
(F. C. Mrazek, J. R. Stapay, J. L. Smith, and T. D. Kaun)

Three 37-mm dia cells (designated 6A, 6B, 8B) were tested for 200 h at 650°C, utilizing a high moisture content (20%) in the electrode gases.* Each cell had a different cathode material--undoped ZnO, $LiFeO_2$, or Li_2MnO_2.

*Anode gas: 0.64 H_2, 0.16 CO_2, and 0.20 H_2O. Cathode gas: 0.53 CO_2, 0.27 O_2, and 0.20 H_2O. Three of the electrode gas flows were monitored throughout the tests by measuring the amount of water loss from the bubbler and the total gas flow.

The open circuit voltages (OCVs) during test were 1.01-1.03 for cell 6A, 0.97-0.98 for cell 6B, and 0.93-0.96 for cell 8B (theoretical OCV = 1.09 with gas-shift equilibrium). These results indicate that some cross leakage had occurred. Disassembly of a cell was done to obtain two cell parts for analysis: a sample of the full electrolyte thickness free of electrode structure, which was used to determine chemically the presence of nonelectrolyte cations, and a cross section of the cell containing the electrolyte and both electrodes, which was used in a microscopic examination.

Results of the quantitative chemical analyses of the electrolyte structures are presented in Table 9. A sample of uncycled electrolyte has also been analyzed to provide a comparative value. The Li_2MnO_3-cathode cell (8B) had a nickel anode substituted for the normally used Ni-10 wt % Cr anode so that the source of chromium contamination in the electrolyte could be easily determined. Table 9 shows a moderate increase of Fe and Cr in all three cells, plus a very large increase of Zn in cell 6A. Earlier solubility measurements determined the solubility of ZnO in Li_2CO_3-K_2CO_3 (eutectic) at 650°C to be 210 wppm.

A test was undertaken to determine whether the $LiAlO_2$ matrix had provided a sink for zinc transported from the cathode into the electrolyte matrix. Sample preparation techniques developed for the ZnO solubility test (above) were employed for selectively dissolving $ZnCO_3$ from samples of the electrolyte structure. This procedure indicated only background levels of zinc, 7.1 wppm. Subsequent treatment of the remaining $LiAlO_2$ with strong acid produced a 2650 wppm level of zinc. These data support the concept of incorporation of ZnO solubility product into the $LiAlO_2$ matrix material.

Cross sections from all three cells were prepared for microscopic examination. No metallic deposit was found in any of the electrolytes from these cells. The electrolyte from the ZnO- and $LiFeO_2$-cathode cells (6A and 6B, respectively) showed the presence of a single, ~0.1-mm thick reddish colored

Table 9. Electrolyte Analyses for Selected Cations

	Contaminants,[a] ppm				
	Fe	Cr	Mn	Ni	Zn
Unused electrolyte	23	<3	4	<3	15
Electrolyte from cell 6A (ZnO cathode)	86	42	29	82	2,940
Electrolyte from cell 6B ($LiFeO_2$ cathode)	170	58	25	4	25
Electrolyte from cell 8B (Li_2MnO_3 cathode)	76	103	24	5	36

[a]Analytical results by E. Huff, ACL.

band, which meandered through the central two-thirds of the 1.4-mm thick electrolyte. This band contains large grains, normally 2-5 μm in diameter, but as large as 25 μm. Examples of these grains are shown in the two SEM photographs of Fig. 16, along with an iron K_α dot map of the single large grain. Energy dispersive spectroscopy (EDS) analysis of the single large grain showed the nonelectrolyte cation to be principally iron, while EDS analysis of the smaller grains showed an approximately equal mixture of iron and chromium, excluding the normally present electrolyte elements. For the colored band in the middle of the cell 6A electrolyte, EDS analysis showed only the presence of chromium, and no unusually high-concentration areas of zinc were observed across the electrolyte thickness. This same sample was submitted to the electron microprobe for zinc analyses at several locations to more clearly define the distribution of the zinc within the electrolyte. A total electrolyte thickness of 1400 μm was analyzed in seven 100-μm bands. Those results are summarized graphically in Fig. 17.* These results, which are semiquantitative because of the lack of a suitable standard, agree well with the bulk chemical analysis value of 0.29 wt % (Table 9).

In cells 6A and 6B the surface of the electrolyte that contacts the Ni-10% Cr anode structure showed the existence of a continuous 30-40 μm-thick gray zone. Analysis by EDS showed the contaminant to be principally chromium. A microsample of this zone, analyzed by X-ray powder diffraction analysis,† showed the contaminant to be similar to $LiCrO_2$ but to have a slightly smaller lattice size. The same sample used for the zinc distribution analyses with electron microprobe was used to determine the amount of chromium in this 30-40 μm layer. Table 10 shows the results of these analyses, using a finely focused beam at seven different locations. These results also are semiquantitative, because of the absence of a suitable standard. This chromium-containing layer appears optically to be at least a two-phase mixture in which chromium-containing crystals are growing within the carbonate-containing

Table 10. Chromium in Anode-Electrolyte Interface Layer

Location	Average Cr/K Ratio × 100
1	30.2 ± 2.1
2	30.8 ± 3.1
3[a]	13.0 ± 1.8
4	36.5 ± 1.1
5	32.4 ± 1.3
6	25.9 ± 4.6
7	33.5 ± 0.8

[a] "Hot spot" of ∿43.6% observed.

*Analysis by C. Seils, CMT.

†Analysis by B. Tani, ACL.

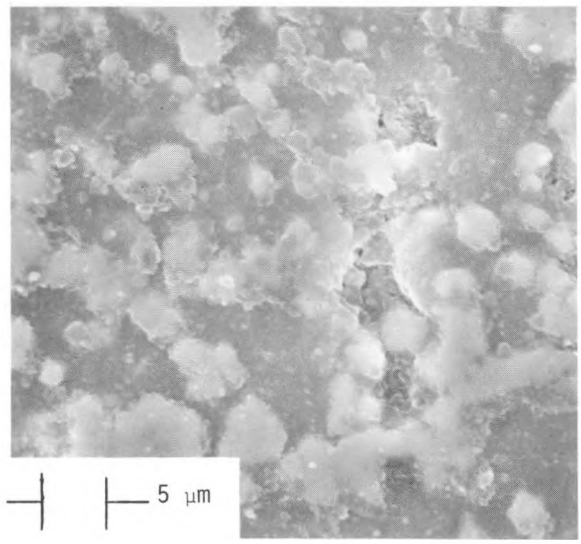

Fig. 16.

SEM of Electrolyte
from Cell 6B

Secondary Electron Image

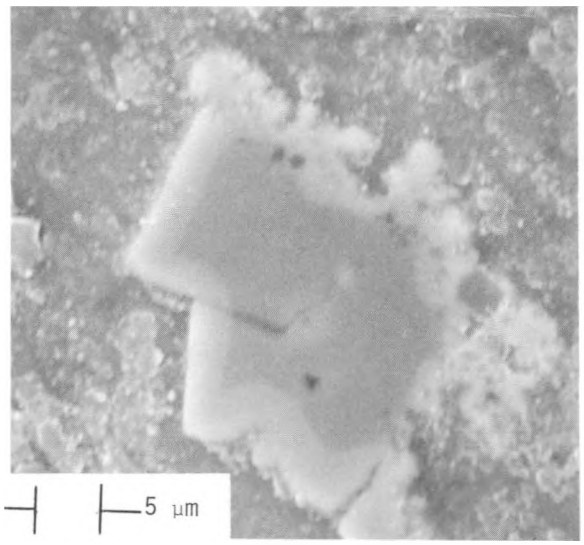

Secondary Electron Image

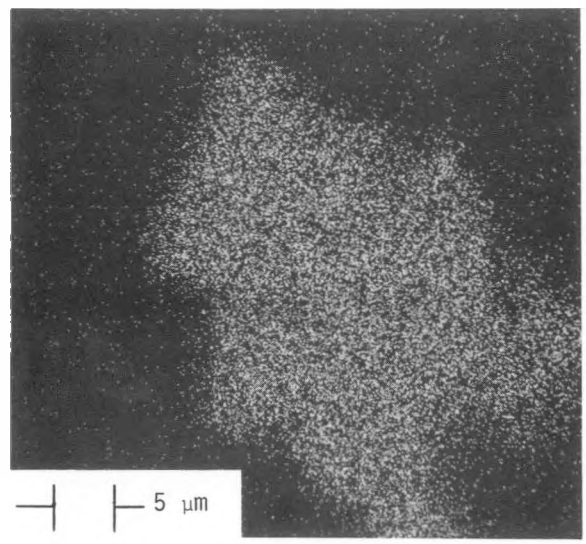

Iron K_α Dot Map of above
Secondary Electron Image

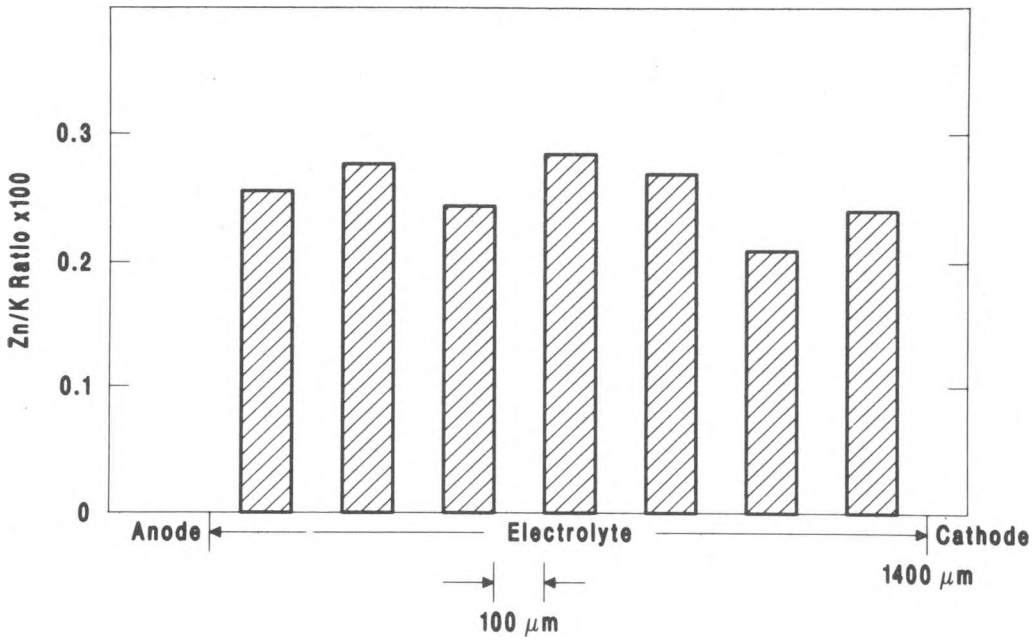

Fig. 17. Zinc Distribution in Electrolyte from Cell 6A

$LiAlO_2$ matrix. If this chromium-bearing compound could be isolated from the electrolyte matrix material, it would show a chromium content of 57 wt %. Since this level of chromium has not been previously observed in the electrolyte at the anode interface in previous cells, it appears that increasing the moisture content of the gases increased the anode corrosion rate.

The last cell examined optically contained the Li_2MnO_3 cathode. A micrograph of the cross section of the entire cell, presented in Fig. 18, shows that both electrodes are in intimate contact with the electrolyte. There is evidence of material fallout from the electrolyte zone during sample preparation, which is usually due to a lower-than-normal carbonate content. Surrounding many of these voids are clusters of large crystals, ranging in size from 20 to 80 μm. Examination of these areas with SEM-EDS suggests that these large crystals (or agglomerates) are the result of $LiAlO_2$ particle growth. This amount of particle growth has not been seen in previous cells. Figure 19 shows an example of these large crystals (or agglomerates), along with high-magnification photographs of both electrodes. As mentioned earlier, the anode in this cell was 100% Ni instead of the normally used Ni-10% Cr. This change resulted in an electrolyte that did not have (1) a "$LiCrO_2$" layer adjacent to the anode and (2) the typical colored band meandering through the electrolyte parallel with the electrodes. This finding appears to confirm that significant chromite solubility occurs at the anode.

Powder X-ray diffraction analysis has been completed on the cathodes from cells 6A and 6B. The $LiFeO_2$ cathode showed a cubic structure with a lattice parameter of 4.158, and the ZnO cathode showed a hexagonal structure with lattice parameter measurements of $a = 3.249$ and $c = 5.205$. The above results are identical to the results obtained on the "starting materials" within the ±0.002 accuracy normally obtained. These results confirm that these cathode compounds are stable under the cell test conditions.

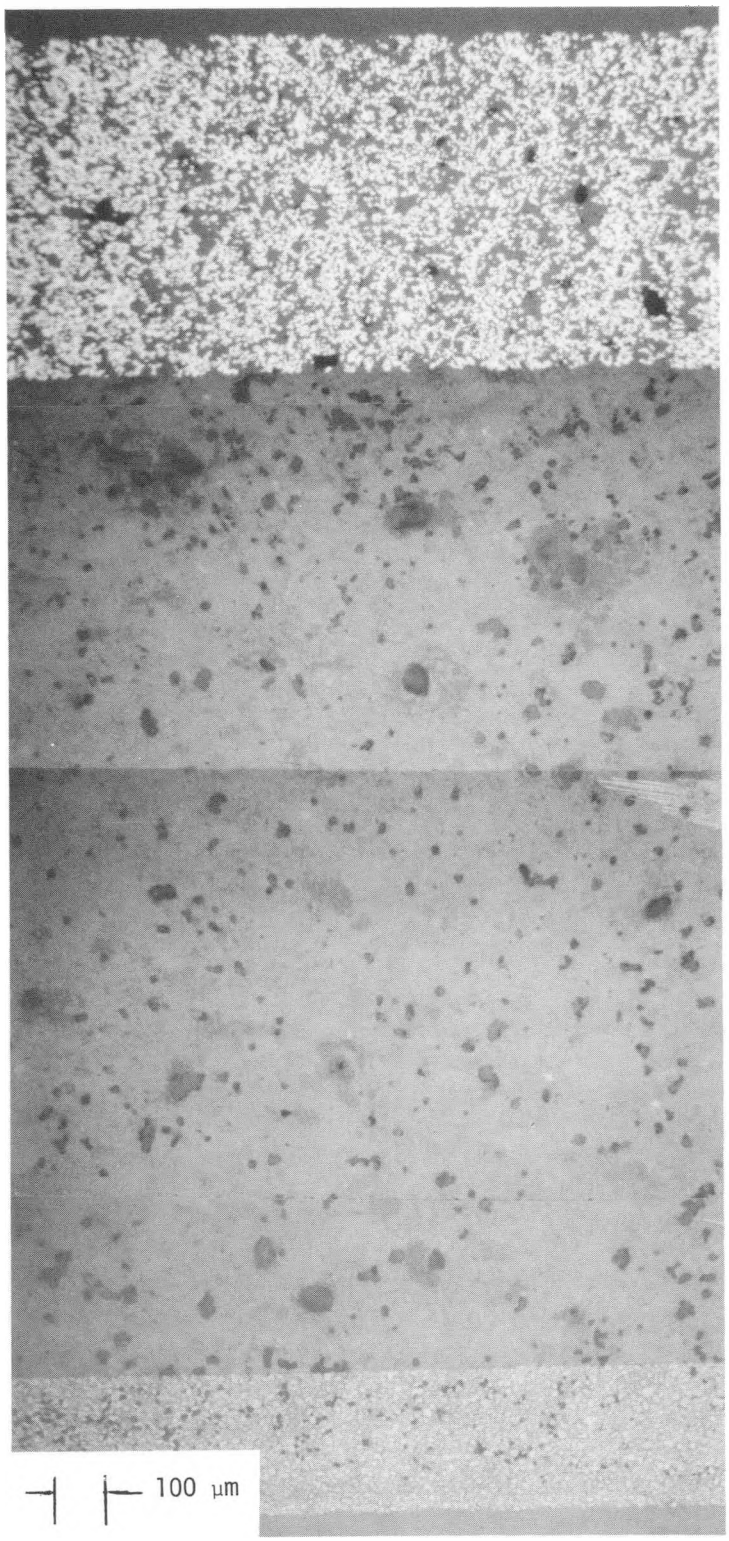

Fig. 18. Full-Thickness Profile of Cell 8B

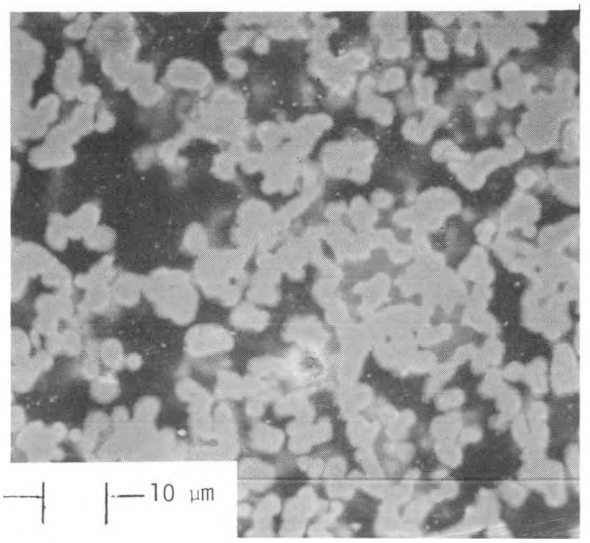

Nickel Anode

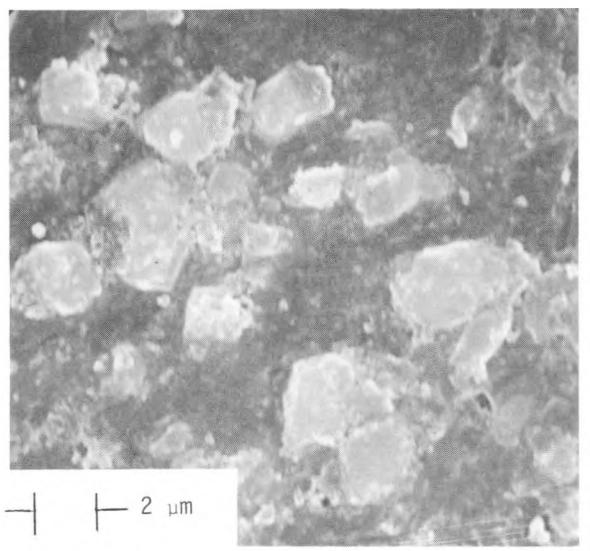

Coarsened Grains of $LiAlO_2$

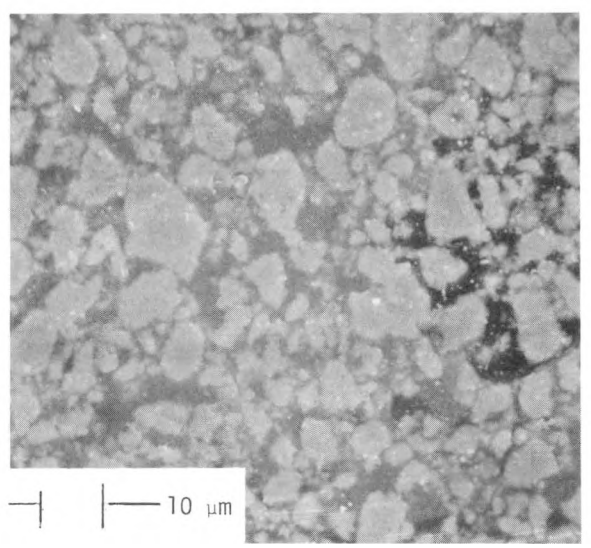

Li_2MnO_3 Cathode

Fig. 19. SEM Photographs of Cell 8B

III. FABRICATION OF CATHODE STRUCTURES
(T. D. Claar, R. J. Fousek, and J. J. Picciolo)*

The objective of this activity is the development of techniques for fabricating alternative cathode materials into thin, porous cathode structures for cell testing. The preliminary cathode specifications are a dual-porosity structure that is approximately 0.4-mm thick and has a total porosity of 55 to 65%. Approximately half of the porosity is to be comprised of small pores (<1 μm) and the balance larger pores (5-10 μm).

Fabrication efforts during the quarter were focused on the synthesis of large batches of alternative cathode material powders and tape casting of thin, porous cathode structures. The current efforts are focusing on Mg-doped Li_2MnO_3, which has shown low electrical resistivity (∿5 ohm·cm at 650°C) and good chemical stability under simulated cathode conditions.

A. Powder Processing

Preparation of the large quantities of alternative cathode powders required for fabrication development is very time-consuming by the present process of coprecipitation followed by solid-liquid separation. Thus, an alternative spray-drying process is being investigated for production of powders for tape-casting fabrication development. The spray drying is being performed in an Anhydro laboratory-scale spray dryer. This unit utilizes a two-fluid nozzle to atomize the feed solution or slurry with compressed air. The feed is atomized countercurrent to the incoming drying air, which is heated electrically.

In the first tests, an aqueous solution of manganese (1 M) and magnesium (0.1 M) nitrates (Mg/Mn molar ratio of 0.1) was prepared and spray dried. With an inlet air temperature of 320°C and outlet temperatures of 110 and 130°C, only a very small amount of powder was collected in the cyclone. Because of the hygroscopic nature of the product nitrates, most of the material stuck to the walls of the dryer. Decreasing the solution feed rate increased the outlet temperature to 160°C and thereby improved the drying efficiency and product yield. Approximately 70 g of a fine, black $(Mg,Mn)(NO_3)_2$ powder (Batch SMM-1) was collected and supplied to J. Smith (CMT) for reaction with 62 mol % Li_2CO_3-38 mol % K_2CO_3 eutectic to form the final Mg-doped Li_2MnO_3 composition. After reaction with molten carbonates, the powder will be washed, filtered, dried, and characterized by X-ray diffraction, chemical analysis, SEM, and electrical resistivity measurement.

In another spray-drying test, Mg-doped Li_2MnO_3 powder was prepared by spray drying a slurry of intimately mixed Li-, Mn-, and Mg-containing precursors, which are subsequently decomposed and reacted at high temperature to form the desired composition and phase assemblage. Such a process would eliminate the time-consuming washing and filtering steps required in the present coprecipitation process. A batch of powder (Batch LMM-1) was prepared by slowly adding an Mn-Mg nitrate solution [2 M $Mn(NO_3)_2$)] with an Mg/Mn ratio of 0.1 to a stoichiometric amount of LiOH aqueous solution (2 M) that contains ∿20% excess hydroxide as NH_4OH, thus coprecipitating Mg and Mn hydroxides. The pH of the resulting slurry changes from about 11 to 9

*Materials Science and Technology Division.

during the course of coprecipitation. The slurry, which had a viscosity of ∿70 cP,* was then spray dried to produce a precursor powder containing Mn and Mg hydroxides and Li nitrate. Approximately 200 g of spray-dried product was collected in the cyclone. The spray-dried powder was heated at 500°C overnight to decompose the nitrate and hydroxides, and then calcined at 1100°C in air for 24 h to form a doped lithium manganate compound. The fired powder was pulverized and screened to -200 mesh. The yield of final powder was 98.4 g, corresponding to ∿41% product yield for the overall process. This relatively low yield was attributed to the use of too large a spraying nozzle, which resulted in inefficient atomization and incomplete drying; thus material stuck to the walls of the dryer.

Examination of the fired LMM-1 powder by SEM showed that the material consists of agglomerates approximately 10 to 30 μm in diameter. These agglomerates have individual particles ∿1 to 3 μm in diameter, which appear to be fairly well sintered together as a result of the 1100°C calcining temperature. Most of the agglomerates contain some microporosity, as shown in the representative SEM micrographs of the fired powder in Fig. 20. X-ray diffraction results indicate that the powder is single-phase monoclinic Li_2MnO_3, whose lattice constants are:

$$a_o = 4.928 \text{ Å}$$

$$b_o = 8.533 \text{ Å}$$

$$c_o = 9.604 \text{ Å}$$

$$\beta = 99.5°$$

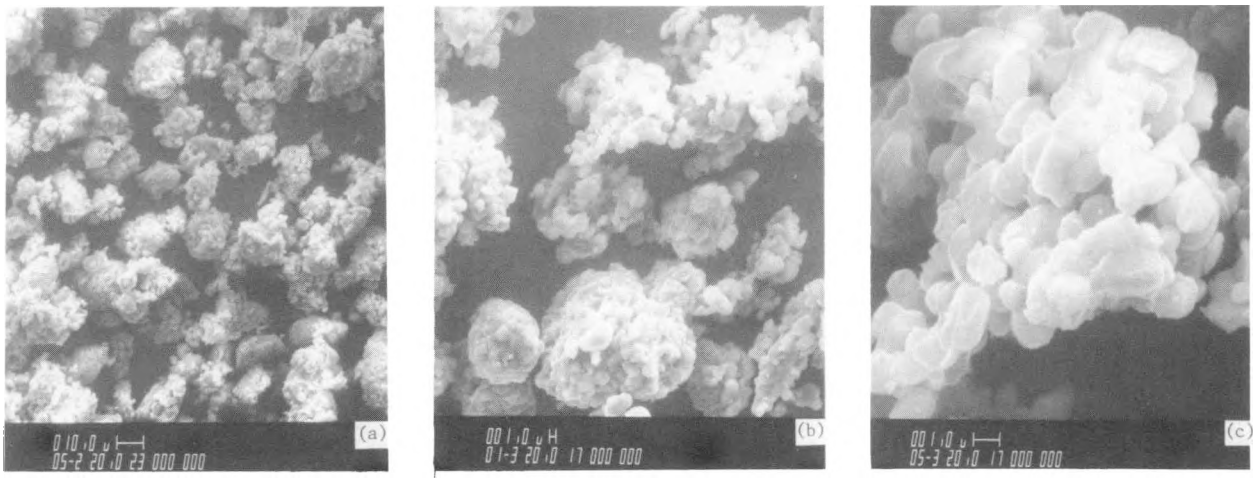

Fig. 20. SEM of Mg-Doped Lithium Manganate Prepared by Coprecipitation and Spray Drying (Batch LMM-1)

*Brookfield Model RVT Viscometer: Spindle #4 at 100 rpm.

The lattice constants of this Mg-doped material were essentially the same as those of pure Li_2MnO_3. The surface area was determined to be 0.09 m^2/g. Chemical analysis results, summarized in Table 11, show that the target dopant level of molar ratio Mg/Mn = 0.1 was achieved.

Table 11. Results of Chemical Analysis of Mg-Doped Li_2MnO_3 Powder LMM-1

Element	Concentration, wt %
Li[a]	11.30
Mn[b]	44.60
Mg[b]	1.99

[a]Atomic absorption spectroscopy.

[b]Ion coupled plasma/atomic emission spectroscopy.

An alternative spray-drying synthesis route was utilized in the preparation of a second batch (LMM-2) of Mg-doped Li_2MnO_3 powder. Stoichiometric amounts of Li_2CO_3, $MnCO_3$, and $Mg(NO_3)_2 \cdot 6H_2O$ were ball milled in distilled water overnight to form a creamy slurry having a viscosity of 290 cP. This slurry was then spray dried at an inlet air temperature of 315°C and outlet temperature of 130°C. Approximately 622 g of product powder was collected from the cyclone. This spray-dried powder was then heated in air at 1000°C for 24 h to react the precursors and form the Mg-doped lithium manganate material. The powder was very flowable after the calcining treatment and passed through a 200-mesh screen without any pulverization. The final product powder yield was 357 g, or approximately 75% for the overall process. Micrographs of the spray-dried and calcined powder LMM-2 are shown in Fig. 21.

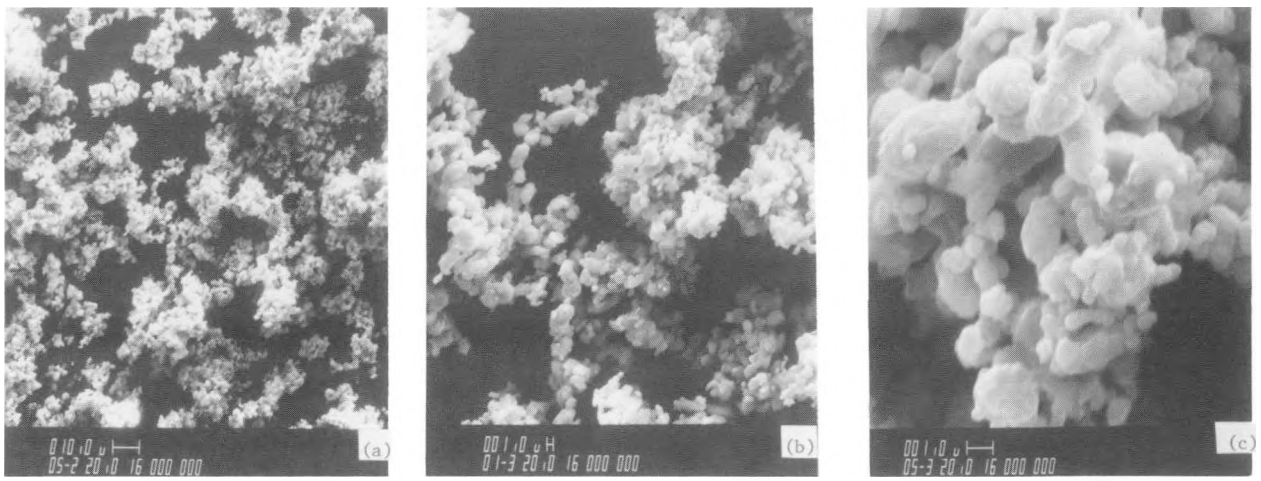

Fig. 21. SEM of Mg-Doped Lithium Manganate Powder Prepared by Spray Drying and Calcining (Batch LMM-2)

Powder Batch LMM-3 was prepared by the process of coprecipitation and spray drying, as described earlier for Batch LMM-1. A smaller spray nozzle was used in the spray drying of Batch LMM-3 in an effort to improve the atomization efficiency of the low-viscosity slurry (∿30 cP) and to increase the product yield. These improvements were attained, as 381 g of product was collected from the cyclone for Batch LMM-3, compared to ∿200 g for Batch LMM-1, for the same amount of feed slurry. The spray-dried powder was heated at 500°C overnight, to decompose the nitrate and hydroxide precursors, then calcined in air at 1000°C for 24 h. Approximately 194 g of final product was obtained, corresponding to a process yield of 82%. About half of the calcined powder was free flowing and could be passed through a 200-mesh screen without pulverization. The remaining powder had sintered into hard agglomerates, which had to be crushed in a mortar and pestle to obtain -200 mesh powder. Powders LMM-2 and -3 are being characterized by chemical, X-ray diffraction, and surface area analyses. Powders have also been submitted to J. Smith (CMT) for electrical resistivity measurements.

B. Tape Casting Development

Development of cathode tape-casting procedures continued during the quarter, using both undoped Li_2MnO_3 powder (Batch 207-151, prepared previously by solid-state reaction of a stoichiometric mixture of Li_2CO_3 and Mn_2O_3) and Mg-doped Li_2MnO_3 powder synthesized by spray drying. Tapes of Li_2MnO_3 were prepared from two different acrylic tape casting binders.* The Cerbind 73150/73151 binder system is formulated to produce green ceramic tapes containing fairly low porosity, while Cerbind 73131 is designed for the fabrication of high-porosity ceramic bodies. The slips were prepared by ball or vibratory milling to wet and disperse the ceramic particles; Z-3 Menhaden fish oil was used as a deflocculating agent. After milling, the slips were partially evacuated to about 400-500 mm Hg vacuum to remove entrained air bubbles. The de-aired slips were cast onto Teflon substrates with a doctor blade set to an opening of 0.75 to 1.0 mm. The dried tapes were very flexible and free of any macrovoids related to entrained air. Slip formulations, preparation procedures, and dried tape thicknesses are summarized in Table 12.

Disk specimens of approximately 2.5-cm dia were punched from selected cathode tapes for organic binder burnout and sintering studies. These specimens were placed on alumina setter plates and heated to 400°C over a period of 10 h for binder burnout, then heated to 1300°C in air and sintered 1 h at this temperature. Geometric densities were calculated from weight, thickness, and diameter measurements taken before and after the sintering treatment; results are summarized in Table 13. The tapes changed in color from orange to black during sintering. The specimens remained reasonably flat and could be handled readily without fracturing.

Tapes made from both the solid-state reaction powder and coprecipitated/spray-dried powder with vibratory-milled slips had green porosities of 58-60% and sintered porosities of ∿32%. In the case of the coprecipitated/spray-dried powder, the milling technique employed had a significant influence on the green and fired densities and resulting microstructure. Because of the

*Cladan Technology, Inc., San Marcos, CA.

Table 12. Summary of Li_2MnO_3 Tape Casting Experiments

Slip No.	Composition	Milling Technique	Tape Thickness, in.[a] As-cast	Tape Thickness, in.[a] Dried
LIM-6	50 g Li_2MnO_3 (207-151) 20 g Cerbind 73151 solution 10 g methylene chloride 34.4 g Cerbind 73150 binder 0.5 g Z-3 fish oil	Vibratory Mill	0.040	0.012-0.013
LIM-7	60 g Li_2MnO_3 (207-151) 60 g Cerbind 73131 binder 0.6 g Z-3 fish oil	Vibratory Mill	0.040	0.015-0.016
LIM-8	40 g Li_2MnO_3-Mg (LMM-1) 40 g Cerbind 73131 binder 0.4 g Z-3 fish oil	Ball Mill	0.030	0.012-0.013
LIM-9	40 g Li_2MnO_3-Mg (LMM-1) 40 g Cerbind 73131 binder 0.4 g Z-3 fish oil	Vibratory Mill	0.030	0.011-0.012

[a]1.000 in. = 25.40 mm.

Table 13. Sintering of Li_2MnO_3 Cathode Tapes[a]

Specimen No.	Powder Batch	Milling	Green Density,[b] % TD	Sintered Density,[b] % TD
LIM-7-2	207-151	Vibratory	42.4	67.6
LIM-8-1	LMM-1	Ball	32.0	45.4
LIM-9-1	LMM-1	Vibratory	40.0	68.9

[a]Disk specimens sintered 1 h at 1300°C in air.

[b]Geometric densities based on theoretical density of 3.80 g/cm^3.

relatively small slip batch sizes used in these tests, ball milling was less efficient than vibratory milling in breaking down agglomerates and dispersing the particles in the slip. As a result, tape LIM-8, made from a ball-milled slip, contained higher green and sintered porosities and larger pores than tape LIM-9, which was cast from a vibratory-milled slip. The effect of the milling procedure on the fired tape microstructure is shown in the SEM micrographs in Fig. 22. It is also apparent from the SEM studies that the micrometer-sized particles present in the spray-dried and calcined powder agglomerates coalesced into 5 to 10 μm particles as a result of the 1300°C sintering treatment, resulting in a loss of surface area and microporosity.

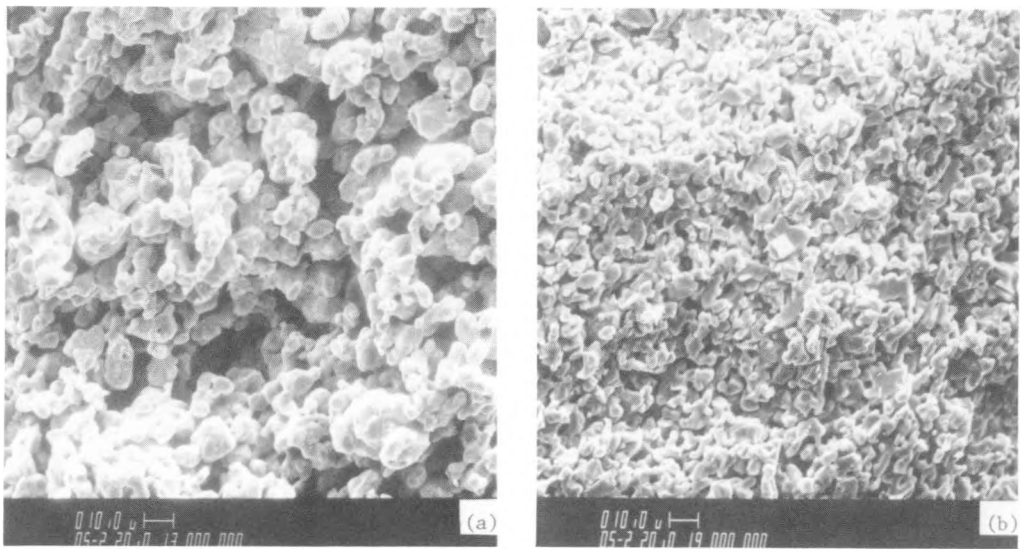

Fig. 22. SEM of Mg-Doped Li_2MnO_3 Tapes Sintered 1 h at 1300°C in Air. (a) Tape LIM-8-1, Ball-Milled Slip; (b) Tape LIM-9-1, Vibratory-Milled Slip.

Further tape casting and sintering studies are in progress. Attempts will be made to produce sintered cathode microstructures containing (1) macropores to aid in gaseous mass transport through the structure and (2) microporosity with associated surface area to support the electrochemical oxygen reduction process at the cathode electrolyte/oxidant three-phase interface. Organic pore formers, such a microcrystalline cellulose, will be investigated as a means of retaining macroporosity in the tape cast and sintered structures. The effect of low sintering temperatures on porosity and microstructure will be established. The feasibility of assembling and testing fuel cells with tape-cast cathodes without sintering will also be assessed.

IV. GAS CLEANUP SYSTEMS ANALYSIS
(H. S. Huang)

In experiments carried out by United Technologies Corp. and the Institute of Gas Technology, it was concluded that molten carbonate fuel cells (MCFCs) can tolerate only limited amounts of sulfur species. In normal MCFC operations, sulfur can enter the cells either with the fuel in the form of H_2S, at a level governed by the extent of the gas cleanup, or with the air, in the form of SO_2, at concentrations up to 40 ppb, depending upon the location. Being an acid, SO_2 would react readily with the molten carbonate electrolyte to form sulfate ions, which, though not harmful to the air electrode, would diffuse towards the fuel electrode. Once in contact with the fuel electrode, sulfate is reduced to sulfide and comes into equilibrium with the gas phase (H_2S) and sulfur adsorbed on the anode. A sulfur loop is formed when the gas stream exiting the anode is burned and then mixed with the incoming air to provide CO_2 and O_2 for the cathodic fuel cell reaction. Any H_2S contained in the anode exhaust stream is converted to SO_2 and returned to the fuel cell via the sulfate transformation route. Consequently, under continuous operation, sulfur would build up in the MCFC until the performance loss would be intolerable. This certainly cannot be permitted to occur, and an approach that will allow at least 40,000 h of satisfactory operation must be taken.

Of the several sulfur-control approaches being proposed, bleeding-off a portion of the anode exhaust gas after combustion seems to be the easiest. Figure 23 is a schematic of this approach for the methane-fueled, internal-reforming MCFC plant. Through this bleed-off, the sulfur cycle is broken

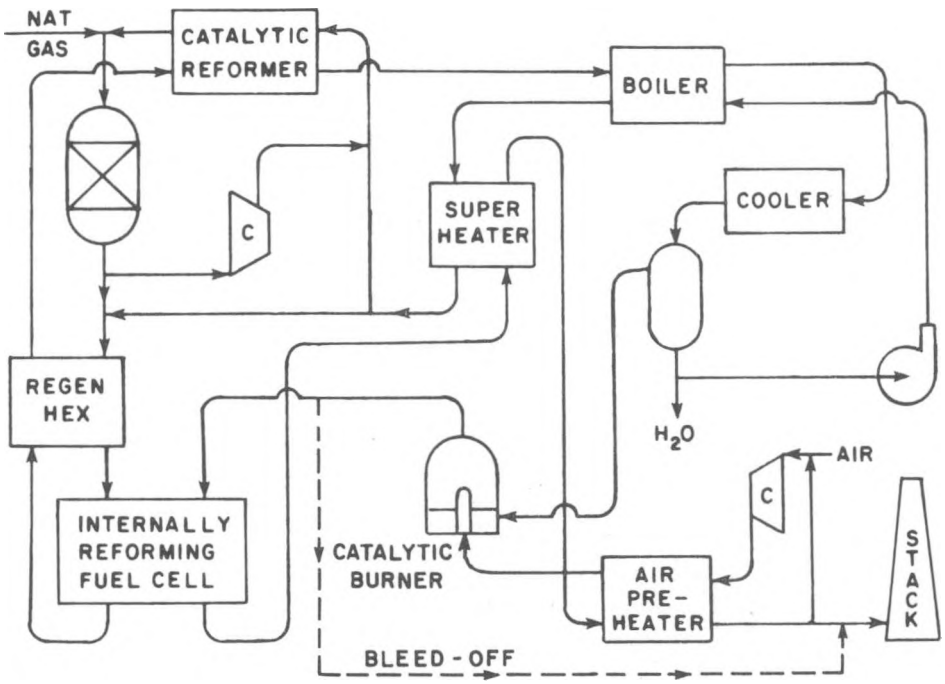

Fig. 23. MCFC Internal-Reforming System (REGEN HEX = regenerative heat exchanger, C = compressor, K.-O. DRUM = knot-out drum)

and continuous sulfur buildup is prevented. However, this simple operation would also cause a decrease in CO_2 concentration in the oxidant gas stream and thereby affect the cell potential, resulting in a decreased overall system efficiency. In addition, the cell potential is adversely affected by the steady-state sulfur levels within the MCFC system. These levels are dictated by the composition of the feeds and the percentage of bleed-off under the bleed-off operating condition. The objective of this task is to carry out a system-performance analysis for a natural gas-based and a coal-based MCFC power plant in which the effectiveness of this bleed-off approach as an alternative sulfur-control measure will be determined.

System performance computations were conducted using SALT code during the quarter for a small MCFC plant (~45 MWe) that is natural-gas fueled and uses internal reforming of methane gas (an Energy Research Corp. innovation). The results are presented in Fig. 24 for the overall plant efficiency as a function of bleed-off ratio and fuel utilization. Table 14 presents the steady-state sulfur levels at various locations within the system for fuel utilization within the cell of 80, 85, and 90% and bleed-offs of 5, 10, and 15%. For the 90% fuel utilization case, satisfactory mass and energy closure could not be attained in cases where the bleed-off ratio was beyond 10% without altering the MCFC operating conditions (mainly the temperatures).

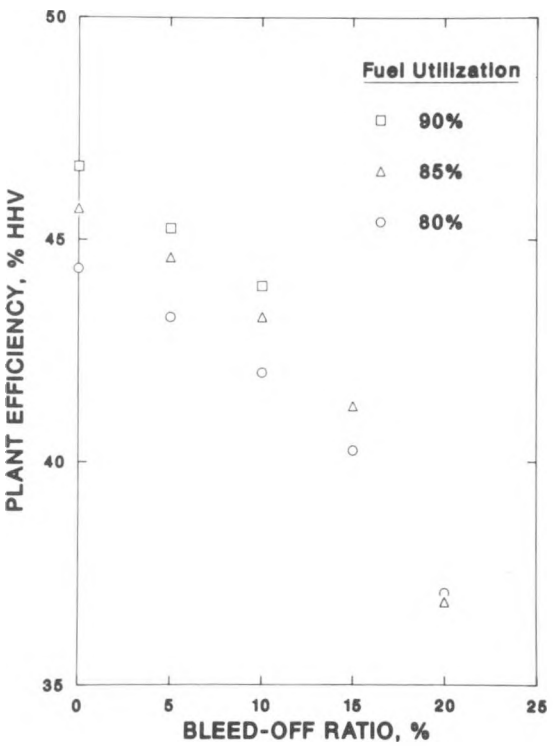

Fig. 24.

Impact of Bleed-Off on MCFC Plant Efficiency (HHV = higher heating value of natural gas)

As evidenced in Fig. 24, the plant efficiency drops significantly as the bleed-off ratio increases, to about 37% with a bleed-off ratio of 20%. For real MCFC operations, a five percentage point decrease in plant efficiency is probably beyond tolerance. This constraint would limit the bleed-off ratio for the natural-gas-based MCFC system to about 15%.

Table 14. Sulfur Concentration within Natural-Gas, Internal-Reforming MCFC

Cases[a]	H_2S in Fuel, ppm	SO_2 in Air, ppm	SO_2 in Cathode Inlet Gas, ppm	H_2S in Anode[b] Exhaust, ppm	H_2S Equiv. in Fuel, ppm
A	0.1	0.00	0.141	0.711	2.000
	0.1	0.01	0.250	1.233	3.469
	0.1	0.02	0.359	1.755	4.938
	0.1	0.03	0.468	2.277	6.407
	0.1	0.04	0.577	2.799	7.876
	0.05	0.00	0.071	0.355	1.000
	0.05	0.01	0.180	0.877	2.469
B	0.1	0.00	0.064	0.355	1.000
	0.1	0.01	0.114	0.601	1.692
	0.1	0.02	0.163	0.847	2.384
	0.1	0.03	0.212	1.093	3.075
	0.1	0.04	0.264	1.339	3.767
	0.05	0.00	0.032	0.178	0.500
	0.05	0.02	0.131	0.669	1.884
C	0.1	0.00	0.038	0.237	0.667
	0.1	0.01	0.068	0.396	1.114
	0.1	0.02	0.098	0.555	1.562
	0.1	0.03	0.128	0.714	2.010
	0.1	0.04	0.158	0.873	2.457
	0.05	0.00	0.019	0.118	0.333
	0.05	0.02	0.079	0.437	1.229
D	0.1	0.00	0.172	0.730	2.000
	0.1	0.01	0.278	1.158	3.173
	0.1	0.02	0.384	1.587	4.346
	0.1	0.03	0.491	2.015	5.519
	0.1	0.04	0.597	2.443	6.692
	0.05	0.00	0.086	0.365	1.000
	0.05	0.01	0.192	0.793	2.173
E	0.1	0.00	0.078	0.365	1.000
	0.1	0.01	0.126	0.568	1.556
	0.1	0.02	0.175	0.771	2.112
	0.1	0.03	0.223	0.974	2.668
	0.1	0.04	0.271	1.177	3.224
	0.05	0.00	0.039	0.182	0.500
	0.05	0.02	0.136	0.588	1.612

(contd)

Table 14. (contd)

Cases[a]	H_2S in Fuel, ppm	SO_2 in Air, ppm	SO_2 in Cathode Inlet Gas, ppm	H_2S in Anode[b] Exhaust, ppm	H_2S Equiv. in Fuel, ppm
F	0.1	0.00	0.046	0.243	0.667
	0.1	0.01	0.076	0.376	1.029
	0.1	0.02	0.105	0.508	1.392
	0.1	0.03	0.134	0.640	1.754
	0.1	0.04	0.164	0.772	2.117
	0.05	0.00	0.023	0.122	0.333
	0.05	0.02	0.082	0.386	1.058
G	0.1	0.00	0.118	0.693	2.000
	0.1	0.01	0.221	1.264	3.649
	0.1	0.02	0.324	1.835	5.299
	0.1	0.03	0.426	2.406	6.948
	0.1	0.04	0.529	2.978	8.598
	0.05	0.00	0.059	0.346	1.000
	0.05	0.01	0.162	0.918	2.649
H	0.1	0.00	0.054	0.346	1.000
	0.1	0.01	0.104	0.639	1.844
	0.1	0.02	0.154	0.931	2.687
	0.1	0.03	0.204	1.223	3.531
	0.1	0.04	0.254	1.515	4.375
	0.05	0.00	0.027	0.173	0.500
	0.05	0.02	0.127	0.758	2.187

[a]Case A = 85% fuel utilization, 5% bleed-off;
Case B = 85% fuel utilization, 10% bleed-off;
Case C = 85% fuel utilization, 15% bleed-off;
Case D = 80% fuel utilization, 5% bleed-off;
Case E = 80% fuel utilization, 10% bleed-off;
Case F = 80% fuel utilization, 15% bleed-off;
Case G = 90% fuel utilization, 5% bleed-off;
Case H = 90% fuel utilization, 10% bleed-off.

[b]It is assumed that all SO_2 in the cathode gas is being absorbed and converted to H_2S at the anode.

Steady-state sulfur levels (Table 14) within the MCFC decrease, as expected, as the bleed-off ratio increases for given sulfur levels in the anode feed stream and air stream. For the 80% and 85% fuel utilization cases, as the background SO_2 concentration in the air increases to 20 ppb and above, the contribution from the air stream to the steady-state sulfur levels will become dominant. This phenomena is even more profound for the 90% utilization case, because of the fact that a greater quantity of air would be required than in the 85% utilization case. The steady-state H_2S

equivalent levels in fuel at the anode inlet are related to the fuel and air streams and the bleed-off ratio by the following expression:

$$XF^{EQ}_{H_2S} = \left(\frac{XF_{H_2S}}{R}\right) + \left(\frac{XA_{SO_2} \cdot MA}{MF}\right)\left(\frac{1 - R}{R}\right)$$

where

XF_{H_2S} = H_2S concentration (in ppm) in fuel,

XA_{SO_2} = SO_2 concentration (in ppm) in air,

MF = fuel molar flow rate,

MA = air molar flow rate,

R = bleed-off ratio

The impact on MCFC operating potential of the varying sulfur levels in both fuel and air streams will be evaluated during the next quarter.

REFERENCES

1. R. Collongues and G. Chaudron, C. R. Acad. Sci. 231, 143 (1950).

2. J. C. Anderson and M. Schieber, J. Phys. Chem. Solids 25, 961 (1964).

3. G. Demoisson, N. Tannieres, C. Gleitzer, and J. Aubry, C. R. Acad. Sci. Ser. C. 274, 1629 (1972).

4. D. D. Wagman, W. H. Evans, V. B. Parker, R. H. Schumm, and R. L. Nuttall, Selected Values of Chemical Thermodynamic Properties, NBS Technical Note 270-8, U.S. Department of Commerce, National Bureau of Standards, p. 21 (1981).

5. I. Barin and O. Knacke, Thermochemical Properties of Inorganic Substances, Springer Verlag, Berlin, p. 432 (1973).

6. T. D. Kaun, "Solubility of the NiO Fuel Cell Cathode in Li_2CO_3-K_2CO_3 Melts as Determined by Cyclic Voltammetry," Extended Abstracts, 163rd Electrochem. Soc. Meeting, San Francisco, CA, May 8-13, 1983, Vol. 83-1, pp. 1155-1156 (1983).

Distribution for ANL-84-38

Internal:

J. P. Ackerman
P. A. Blackburn
R. L. Breyne
L. Burris
T. D. Claar
G. M. Cook
D. W. Dees
J. T. Dusek
D. C. Fee
P. A. Finn
B. K. Flandermeyer
A. V. Fraioli
J. E. Harmon
A. A. Jonke
T. D. Kaun
V. M. Kolba
T. E. Kraft
M. Krumpelt
G. H. Kucera
N. Q. Minh
F. C. Mrazek
Z. Nagy
P. A. Nelson
J. J. Picciolo
R. D. Pierce (25)
R. B. Poeppel
J. J. Roberts
J. L. Smith
J. R. Stapay
R. K. Steunenberg
B. S. Tani
E. H. VanDeventer
J. E. Young
S. A. Zwick
A. B. Krisciunas
ANL Patent Dept.
ANL Contract File
ANL Libraries (3)
TIS Files (6)

External:

DOE-TIC, for distribution per UC-93 (126)
Manager, Chicago Operations Office, DOE
R. J. Gariboldi, DOE-CH
F. Herbaty, DOE-CH
M. Zahid, DOE-CH
Chemical Technology Division Review Committee Members:
- S. Baron, Burns and Roe, Inc., Oradell, N. J.
- W. L. Worrell, U. Pennsylvania
- E. B. Yeager, Case Western Reserve U.

Materials Science Division Review Committee:
- C. B. Alcock, U. Toronto
- A. Arrott, Simon Fraser U.
- R. C. Dynes, Bell Labs., Murray Hill
- A. G. Evans, U. California, Berkeley
- H. K. Forsen, Bechtel Group, Inc., San Francisco
- E. Kay, IBM San Jose Research Lab.
- M. B. Maple, U. California-San Diego
- P. G. Shewmon, Ohio State U.
- J. K. Tien, Columbia U.
- J. W. Wilkins, Cornell U.

B. S. Baker, Energy Research Corp., Danbury, Conn.
R. W. Barta, General Electric Co., Ballston Spa, N. Y.
L. J. Bates, Battelle Pacific Northwest Lab.
T. R. Beck, Electrochemical Technology Corp., Seattle
A. Boni, Physical Sciences, Inc., Andover, Mass.
R. Bradley, Oak Ridge National Lab.
E. Camara, Inst. Gas Technology, Chicago
P. T. Carlson, Oak Ridge National Lab.
T. W. Carter, U. S. Coast Guard, Washington
D. Chatterji, General Electric Co., Schenectady
J. Cuttica, Gas Research Inst., Chicago
W. Feduska, Westinghouse R&D Center, Pittsburgh
L. M. Ferris, Oak Ridge National Lab.
A. P. Fickett, Electric Power Research Inst.
E. Gillis, Electric Power Research Inst.

J. Giner, Giner, Inc., Waltham, Mass.
F. Gmeindl, Morgantown Energy Technology Center
G. L. Hagey, Div. Advanced Energy Conversion Systems, USDOE
J. W. Harrison, General Electric Co., Wilmington, Mass.
L. C. Headley, Morgantown Energy Technology Center
D. T. Hooie, Gas Research Inst., Chicago
W. Huber, Morgantown Energy Technology Center
A. O. Isenberg, Westinghouse R&D Center, Pittsburgh
B. Jackson, Tennessee Valley Authority, Chattanooga
D. Johnson, Northwestern U.
C. Kinney, Office of Fossil Energy, USDOE
K. Kinoshita, Lawrence Berkeley Lab.
M. Kresge, Mitsubishi International Corp., New York City
H. R. Kunz, United Technologies Corp., South Windsor, Conn.
A. R. Maret, Gas Research Inst., Chicago
N. Margalit, Combustion Engineering, Windsor
L. Marianowski, Inst. of Gas Technology, Chicago
H. Maru, Energy Research Corp., Danbury, Conn.
R. Matsumato, Ceramatech, Salt Lake City
A. P. Meyer, United Technologies Corp., South Windsor, Conn.
C. A. Reiser, United Technologies Corp., South Windsor, Conn.
F. Salzano, Brookhaven National Lab.
J. Searls, U. S. Bureau of Mines, Washington
R. Selman, Illinois Inst. of Technology
J. Sholes, Morgantown Energy Technology Center
P. Stonehart, Stonehart Associates, Inc., Madison, Conn.
G. Wilemski, Physical Sciences Inc., Andover, Mass.
C. Zeh, Morgantown Energy Technology Center, USDOE